Modeling in Support of Lower Hybrid Current Drive Experiments on the EAST Tokamak

P. T. Bonoli[1], S. G. Baek[1], D. B. Batchelor[2], B. Ding[3], J. P. Lee[4], M. Li[3], S. Shiraiwa[1], J. C. Wright[1] and C. Yang[3]

[1]MIT-PSFC, Cambridge, MA 02139

[2]D. B. Batchelor, DIDITCO, Knoxville, TN 37919

[3]CAS-IPP, Hefei, China

[4]Hanyang University, Seoul, 04763, Korea

9th US-PRC Magnetic Fusion Collaboration Workshop

June 5-7, 2018

MIT Plasma Science & Fusion Center

Modeling and simulation is aimed at understanding the role of full-wave effects and parasitic losses in the SOL in LHCD experiments in EAST

- Use coupled full-wave / Fokker Planck simulations to understand the regimes where ray tracing approach is valid.

- Develop reduced model for LHCD actuator that is usable in control level Plasma Control System algorithms and fast transport solvers.

- Evaluate the effect of increasing LH source frequency on nonlinear parametric decay instability in the SOL.

LHCD in the EAST Tokamak

- **LHCD experiments in EAST are in the weak damping regime where full-wave effects and interference effects can potentially be important [1, 2]:**

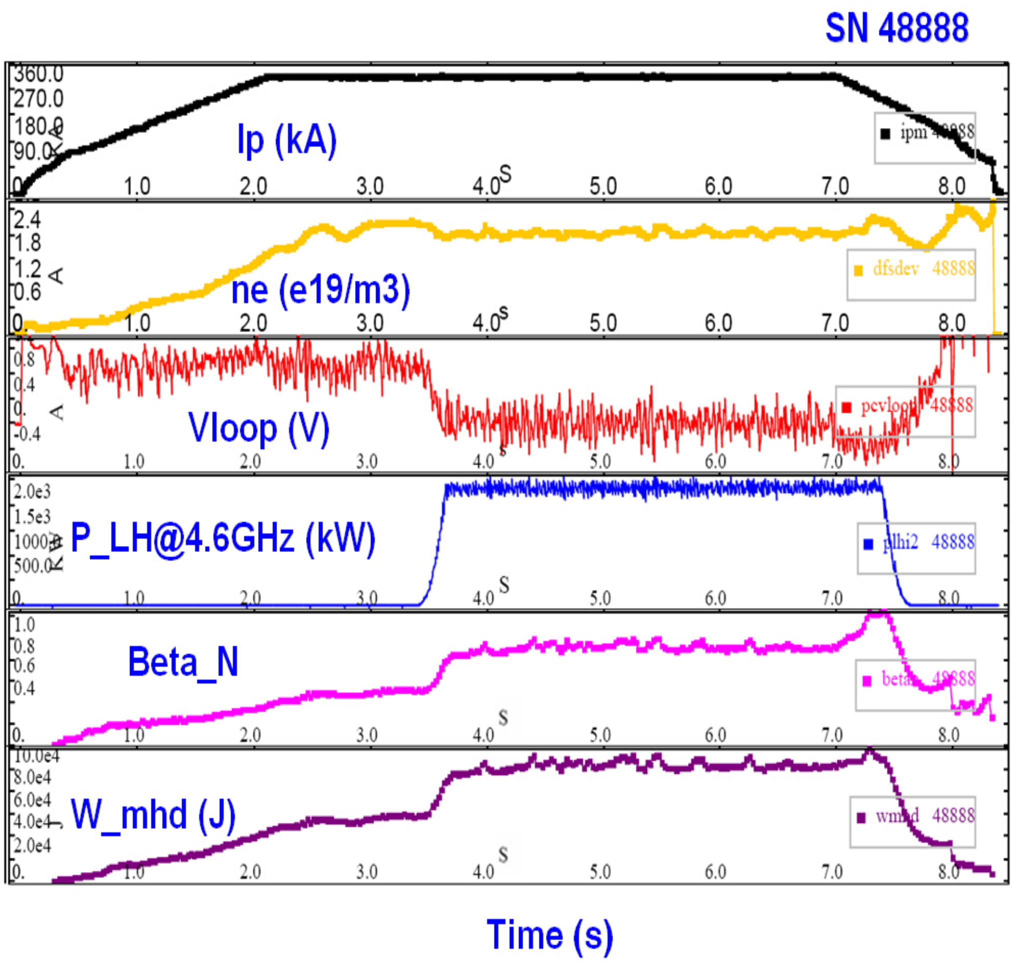

Ray tracing / Fokker Planck simulations using GENRAY / CQL3D [3,4] over-estimate driven LH current with completely hollow profiles

Ray launched from all 12 rows

Launcher spectrum ($N_{//}$ =2.05, -6)

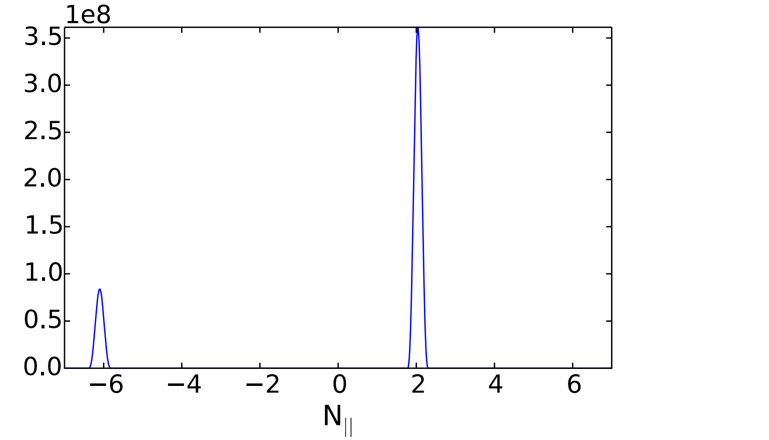

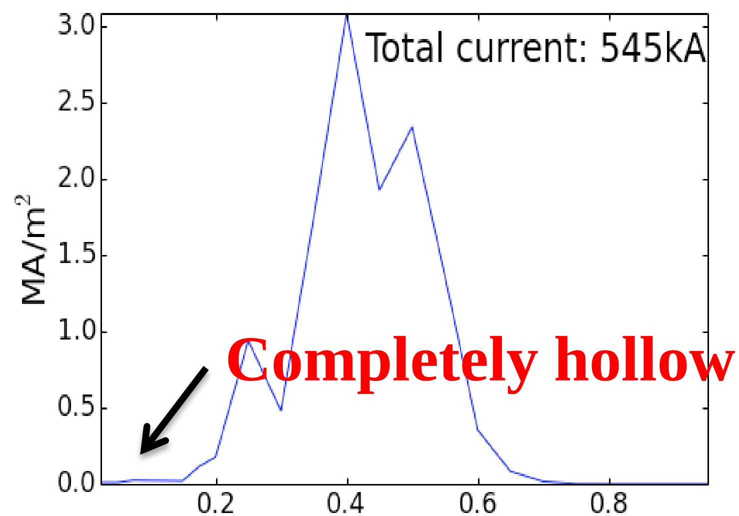

Set-up for TorLH full-wave simulations

- **Use experimental profiles and EFIT equilibrium reconstruction for discharge 048888.05500:**
  - B_0 = 2.31 T, I_p = 373 kA, a = 0.42 m, R_0 = 1.85 m, $T_e(0)$ = 3.2 keV, $n_e(0) = 3.6 \times 10^{19}$ m^{-3}.

- **RF parameters:**
  - P_{LH} = 2 MW, f_0 = 4.6 GHz, $n_{//}$ = -1.80

- **Status of TorLH [1], GENRAY [3], and CQL3D [4] executables:**
  - NERSC: Edison
  - MIT-PSFC Engaging Cluster
  - IPP Shenma Cluster

Numerical implementation and mode resolution requirements for TorLH

- **Semi-spectral ansatz is assumed for the electric field:**

$$\vec{E}(\vec{x}) = \sum_{m,n} \vec{E}_{m,n}(\psi) e^{im\theta + in\phi}$$

  - Spectral decomposition in the poloidal (*m*) and toroidal (*n*) directions.
  - $E_{m,n}(\psi)$ are represented by finite elements in the radial direction (cubic Hermite interpolating polynomials).

- **Using the ansatz above, the wave equation can be put in a weak variational form (Galerkin method):**
  - Each toroidal mode (*n*) is solved separately assuming N_m poloidal modes and N_r radial elements.
  - **This results in a block tri-diagonal matrix to invert [5].**

Poloidal mode resolution requirements for TorLH to simulate LH wave propagation in EAST

- **Must resolve the shortest perpendicular wavelength in the system, which is given by the LH dispersion relation:**

$$k_\perp \approx k_{//}\frac{\omega_{pe}}{\omega} \approx \frac{m}{r}$$

- **For an EAST discharge at r/a ~ 0.5 with B_0 = 2.3 T, $T_e(0)$ ~ 1 keV, $n_e(0) \sim 2.0 \times 10^{19}$ m^{-3}, f_0 = 4.6 GHz, we have:**

$$k_\perp = 17\ cm^{-1}\ (\text{for } n_{//}\sim \mathrm{n}_{//0}=2) \Rightarrow m \approx rk_\perp \approx 372$$
$$\text{and } N_m = 2m+1 = 745$$

$$k_\perp = 46\ cm^{-1}\ (\text{for } n_{//}\sim \mathrm{n}_{//ELD}\sim 5.5) \Rightarrow m \approx rk_\perp \approx 1019$$
$$\text{and } N_m = 2m+1 = 2038$$

- **May need N_m ~ 4000 to resolve LH wave at edge ~ 45 cm.**

Convergence is only achieved on innermost flux surface (r/a ≈ 0.1) at N_m = 255

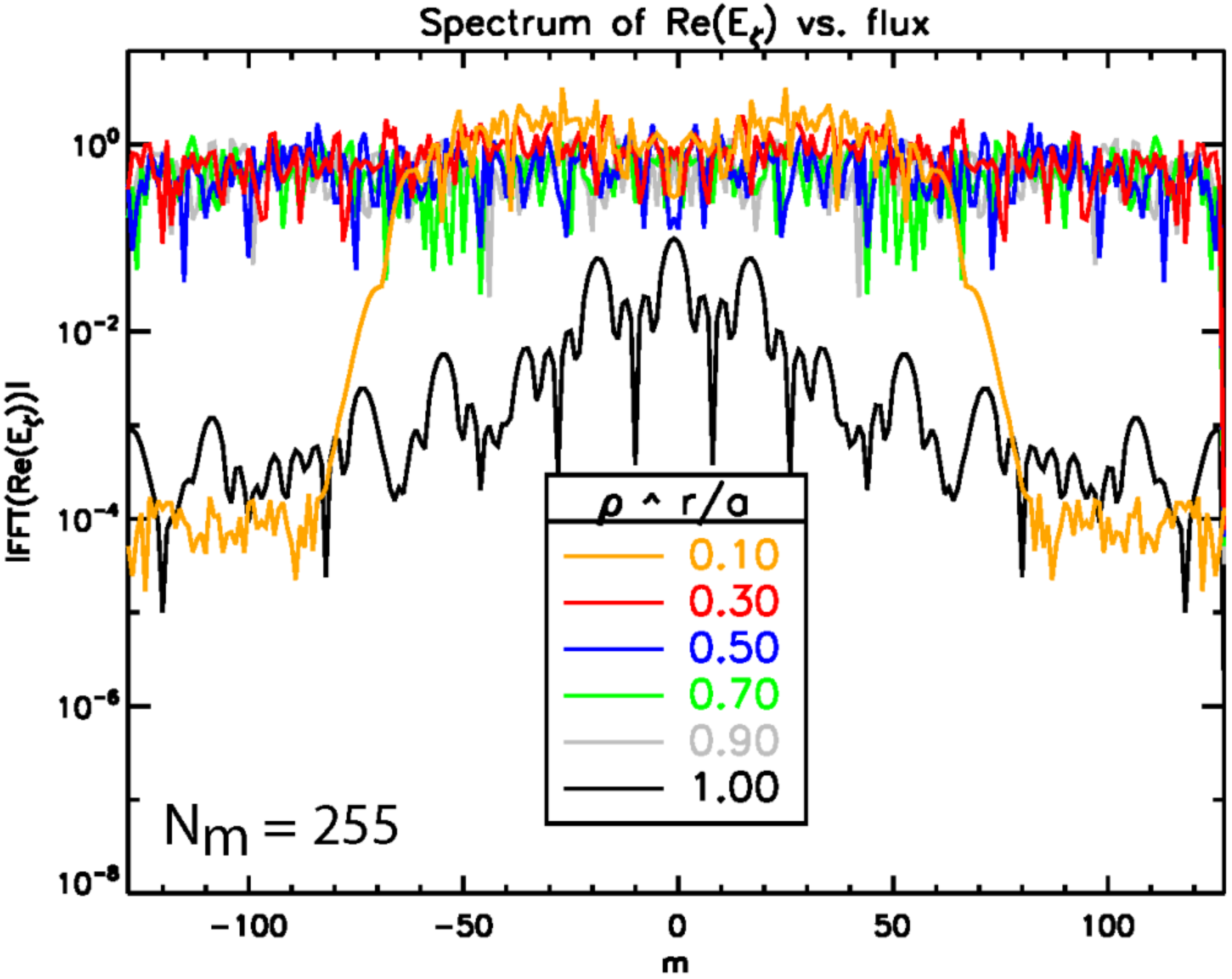

Convergence continues to improve on flux surfaces out to r/a ≈ 0.5 as N_m is increased to 2047

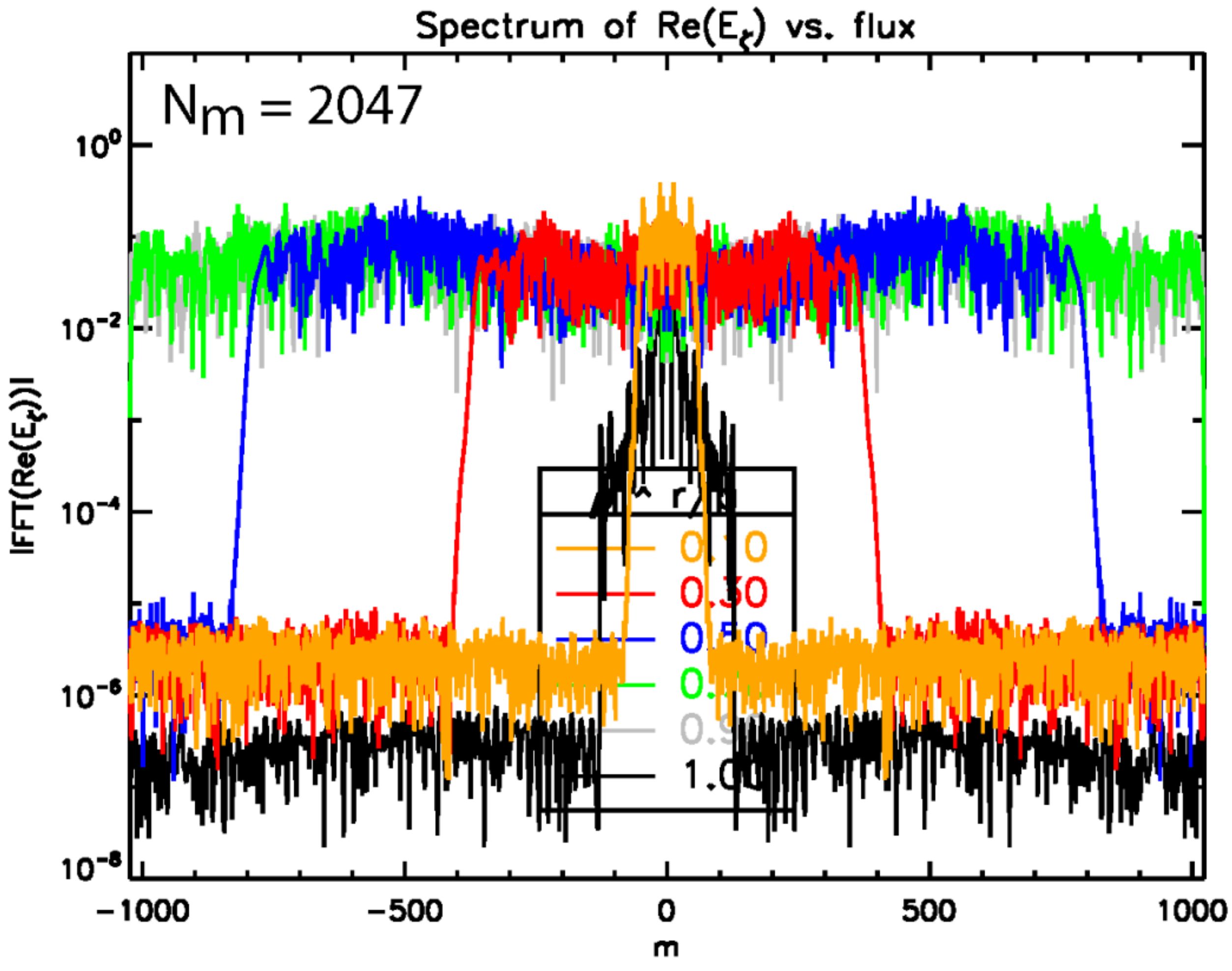

Find that convergence is achieved on all flux surfaces as N_m is increased to 4095

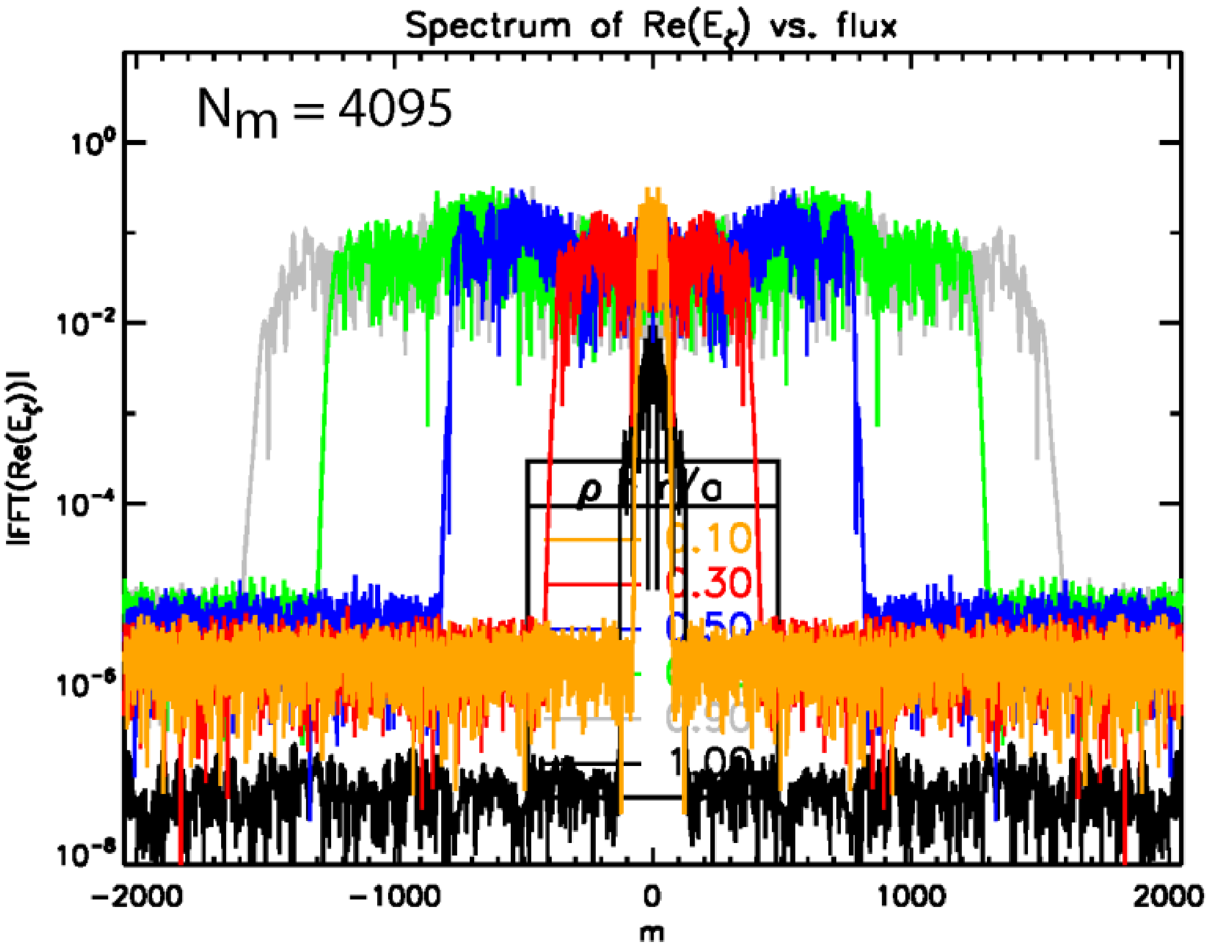

- **Simulation required 0.57 hours of wall clock time on Edison platform at NERSC using 32,256 cores**

LH power deposition profile is peaked on-axis at N_m = 255, but starts to broaden as N_m is increased

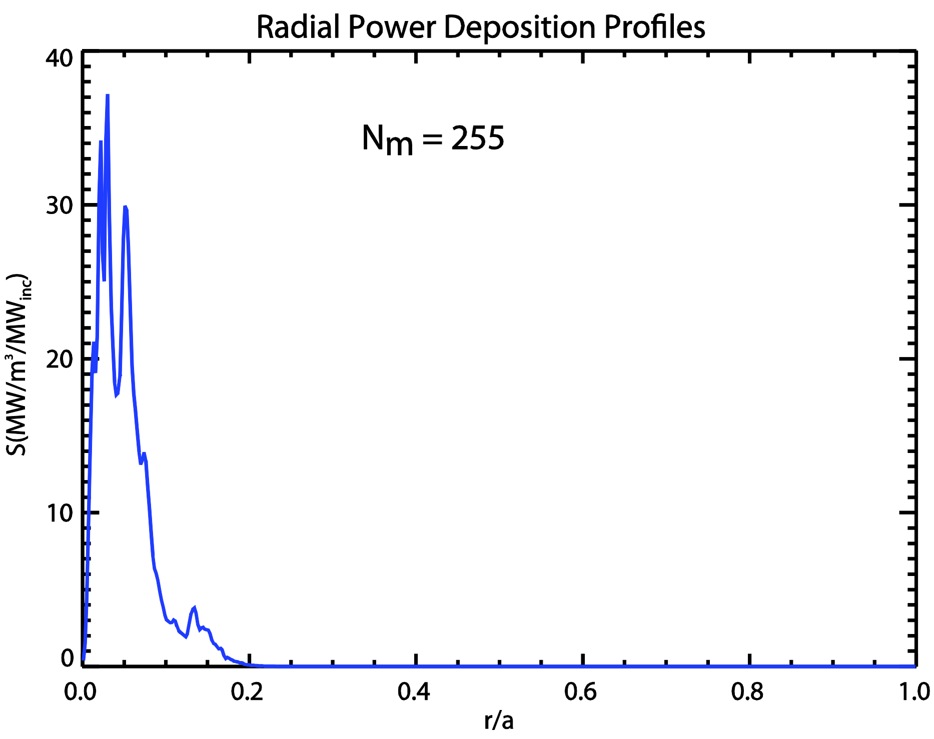

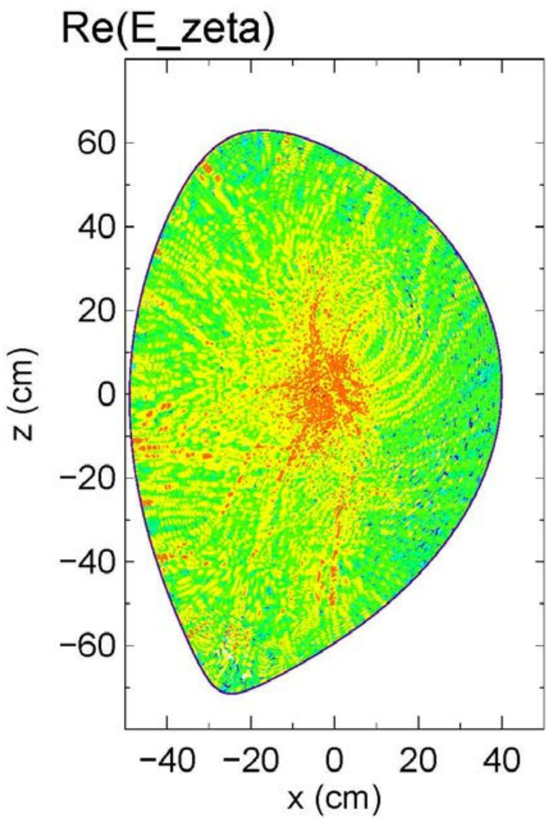

- **Broadening of the LH power deposition profile is consistent with adding higher $k_{//}$ components to the spectral solution in TorLH that correspond to higher m.**

At N_m = 4095 the full-wave absorption profile is clearly off-axis (for Maxwellian electron damping)
→ consistent with ray tracing prediction

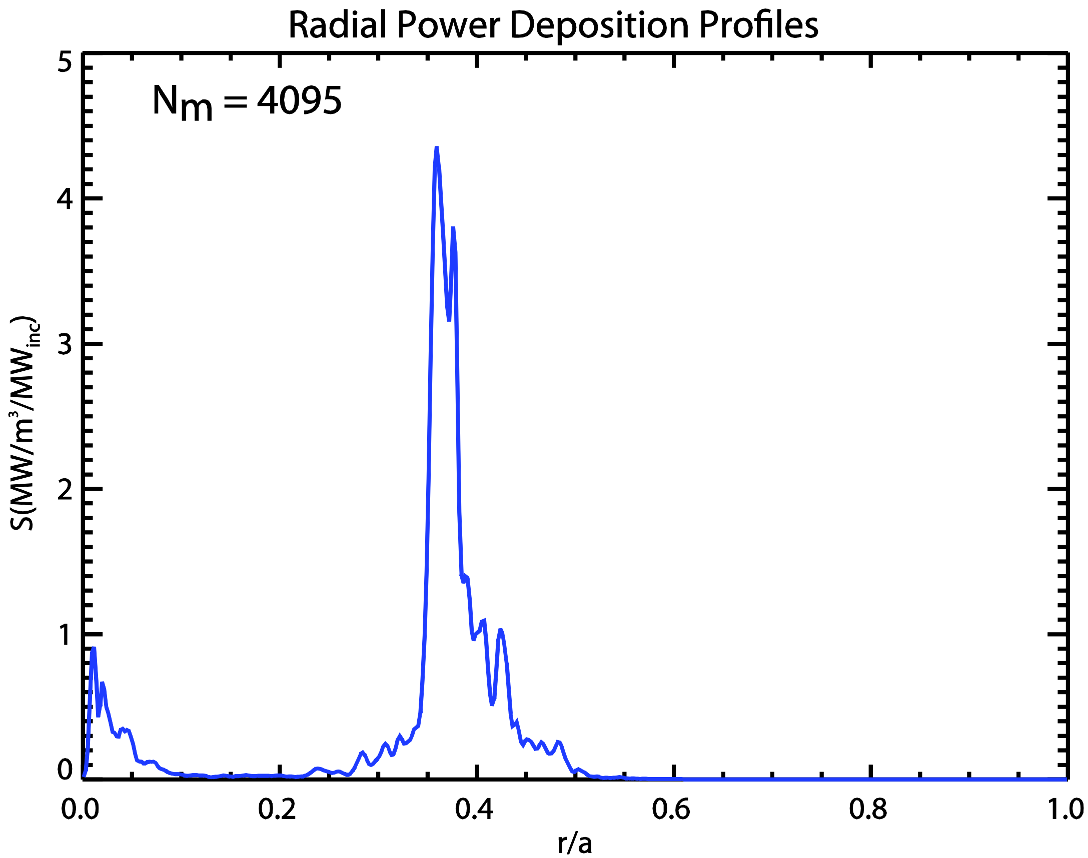

N_m = 4095

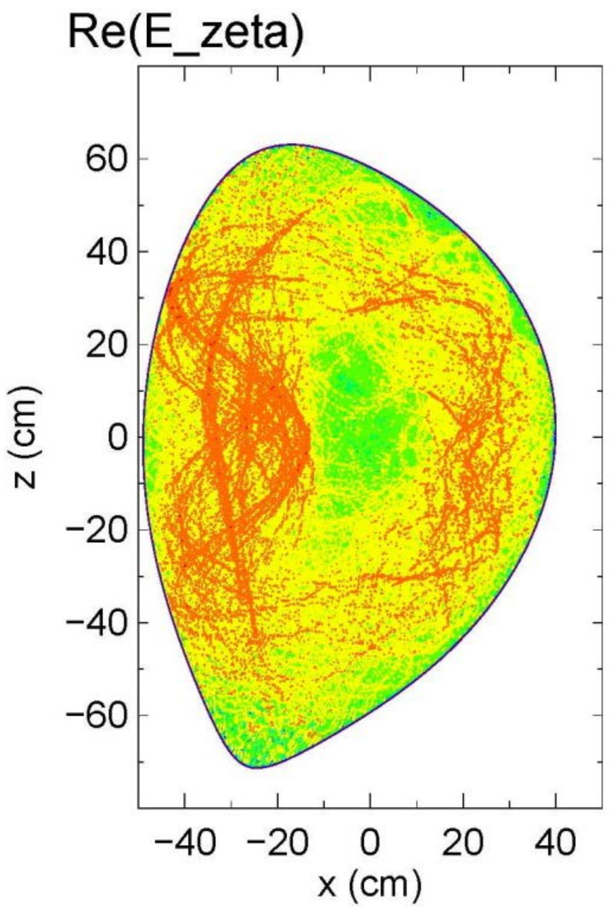

Workflow for TorLH-CQL3D simulation has been automated using the Integrated Plasma Simulator (IPS)

a) Execute TorLH in "toric" mode using Maxwellian electron Landau damping (ELD):

   i. Perform a resolution scan to determine how many poloidal modes are needed to resolve the LH wave in EAST.

b) Re-run TorLH in "qldce" mode to compute the RF diffusion coefficients (D_ql) from the electric field solutions computed in Step (a):

   i. Remap D_ql from the TorLH (radial, velocity) space mesh to the CQL3D (radial / velocity) space mesh.

c) Run CQL3D to obtain first iterate for the quasilinear electron distribution $f_e(v_\perp, v_{//}, r)$:

   i. Create look-up table for $Im\{\chi_{zz}\}$ due to ELD.

d) Repeat steps (a) – (c) until $f_e(v_\perp, v_{//}, r)$ and D_ql (f_e) are self-consistent.

TorLH - CQL3D has been iterated to convergence using the IPS with 1023 poloidal modes

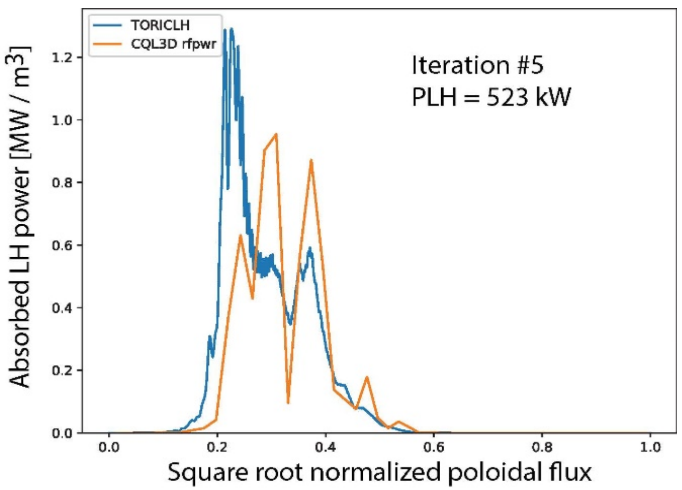

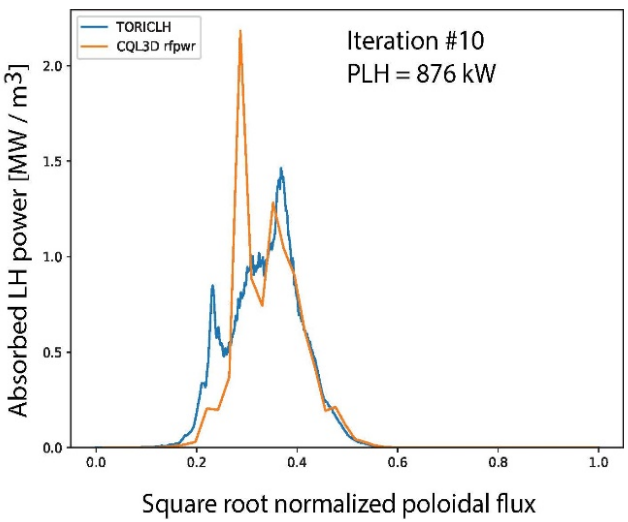

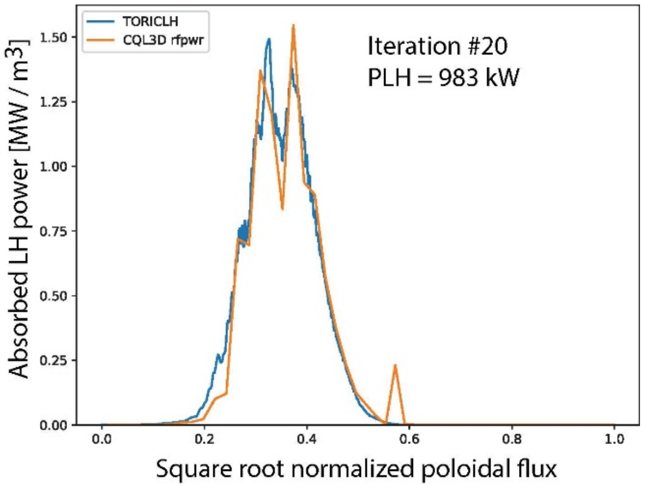

Agreement in profiles of LHRF power deposition from TorLH and CQL3D indicate convergence

TorLH - CQL3D has been iterated using the IPS with 4095 poloidal modes for 5 iterations

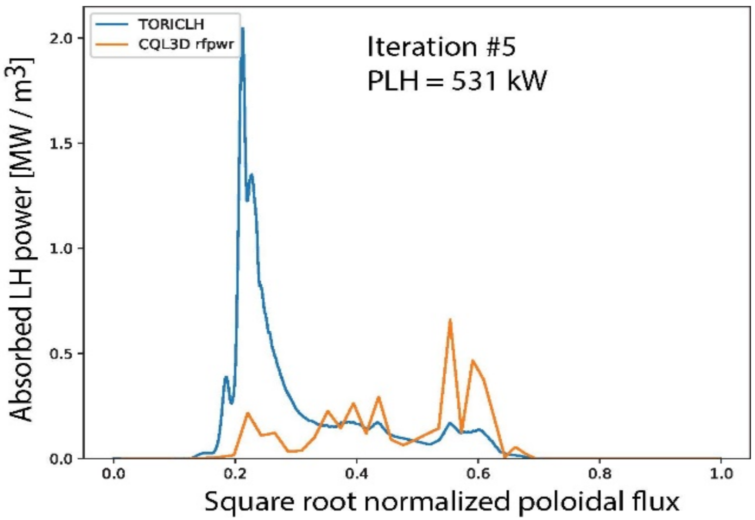

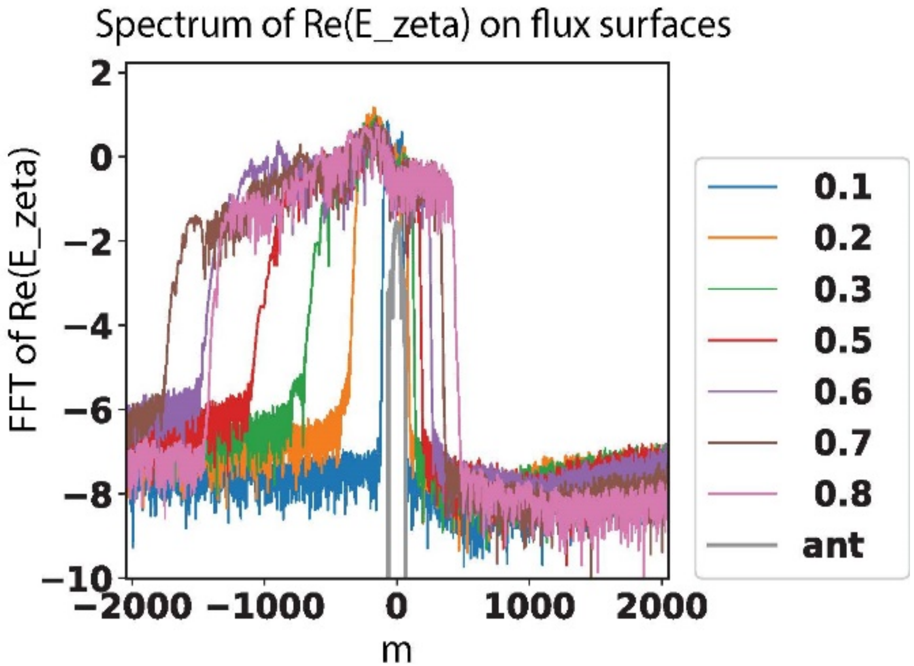

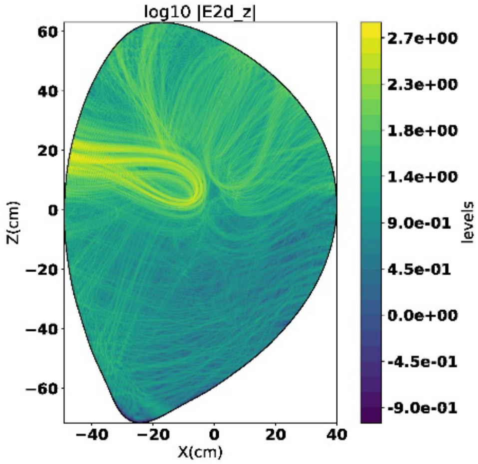

Simulation starting to exhibit features of convergence but must be extended to 15-20 iterations.

Developing a control level model for LHCD using GENRAY / CQL3D

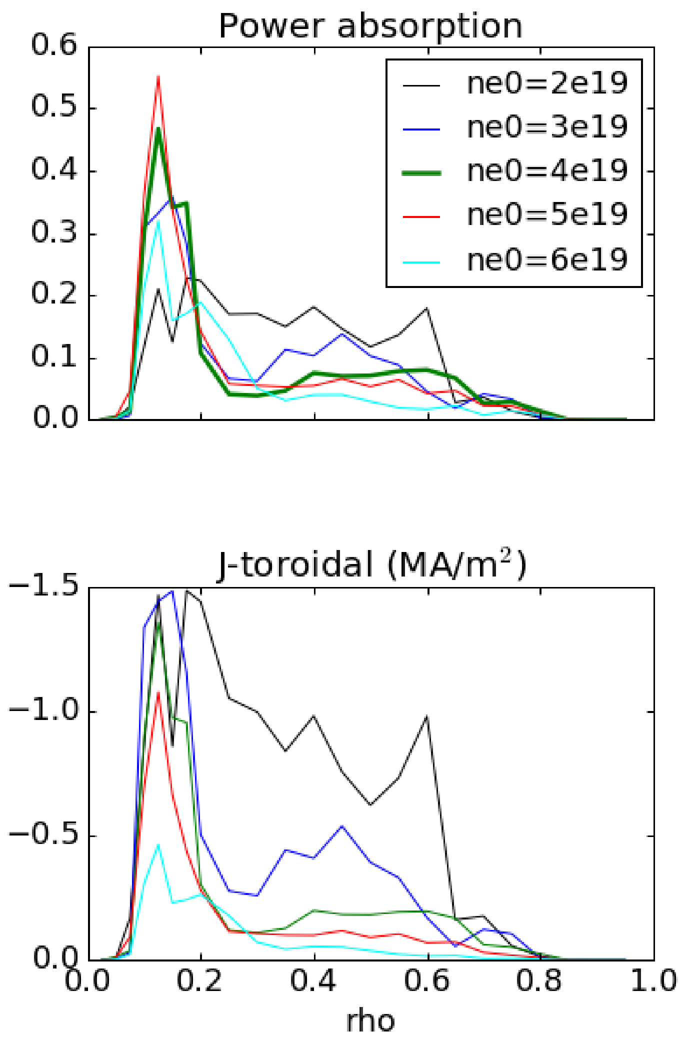

- **Must reduce the hyper-sensitivity of LHCD prediction.**
- **Broadening of LH wave spectrum is introduced:**
  - **Phenomenological model of wave scattering due to density fluctuation (Note this model is experimental)**
- **Initial result is promising, reducing the variation of predicted profiles.**

Previous data show off-axis peaks at large rho

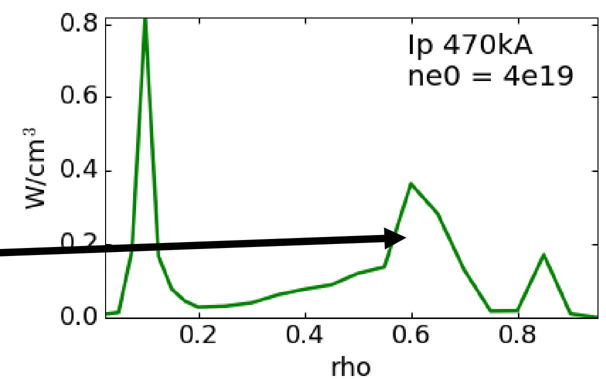

Development of a LH wavenumber measurement system for EAST is near completion (see poster by M. Li)

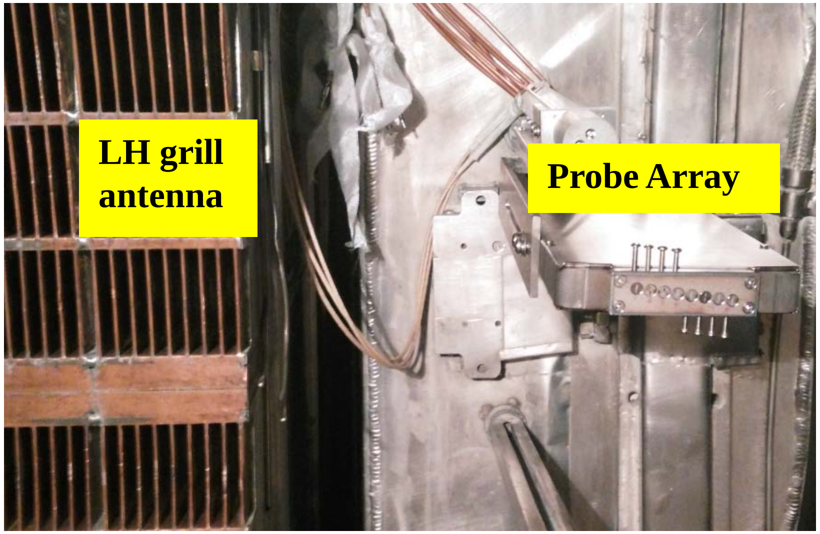

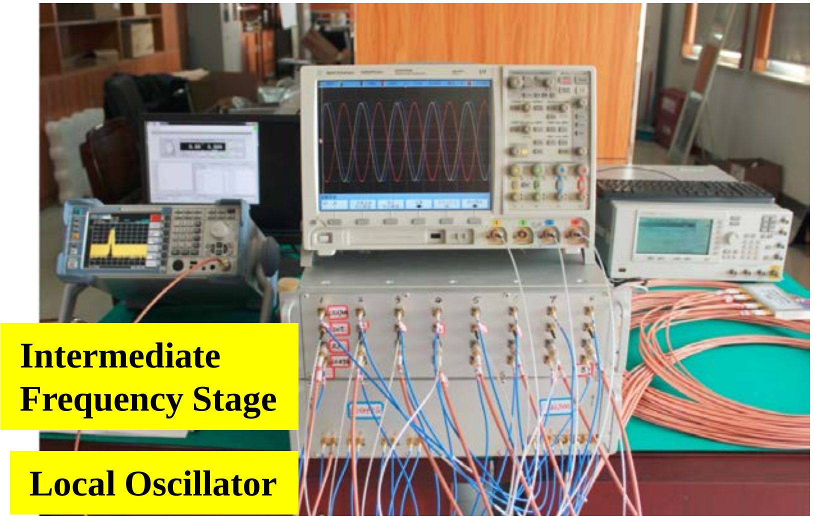

The LH magnetic loop probes are installed next to the 4.6 GHz antenna to detect the wave-field on the first pass to the plasma.

The intermediate frequency stage down-converts the wave frequency from 4.6 GHz to 20 MHz, allowing to perform FFT analyses.

Initial measurement of the frequency spectrum at 4.6 GHz shows the absence of the PDI sideband at $\bar{n}_e$ = 3x10^{19} m^{-3} (see poster by M. Li)

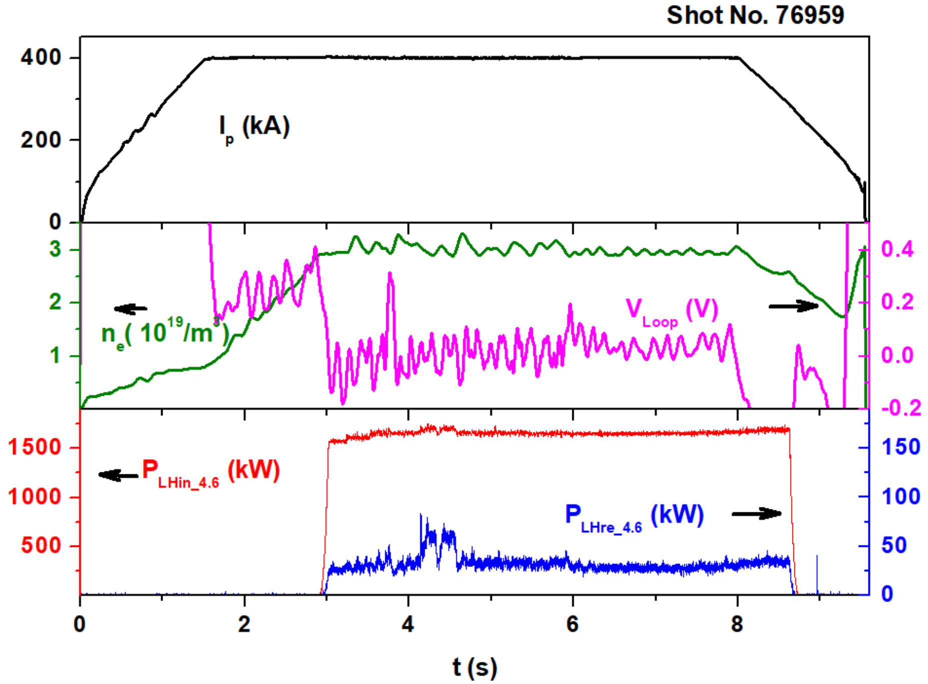

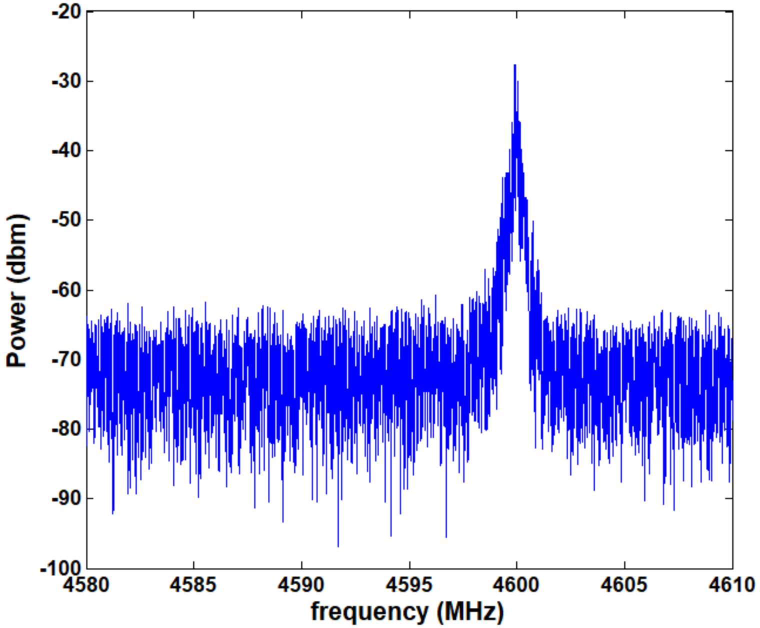

Upon the completion of the diagnostic, the wave $k_{//}$ spectrum will be examined under various plasma conditions in the up-coming campaign.

Parametric dispersion relation analysis indicates reduced growth rates for decay waves at 4.6 GHz relative to 2.45 GHz

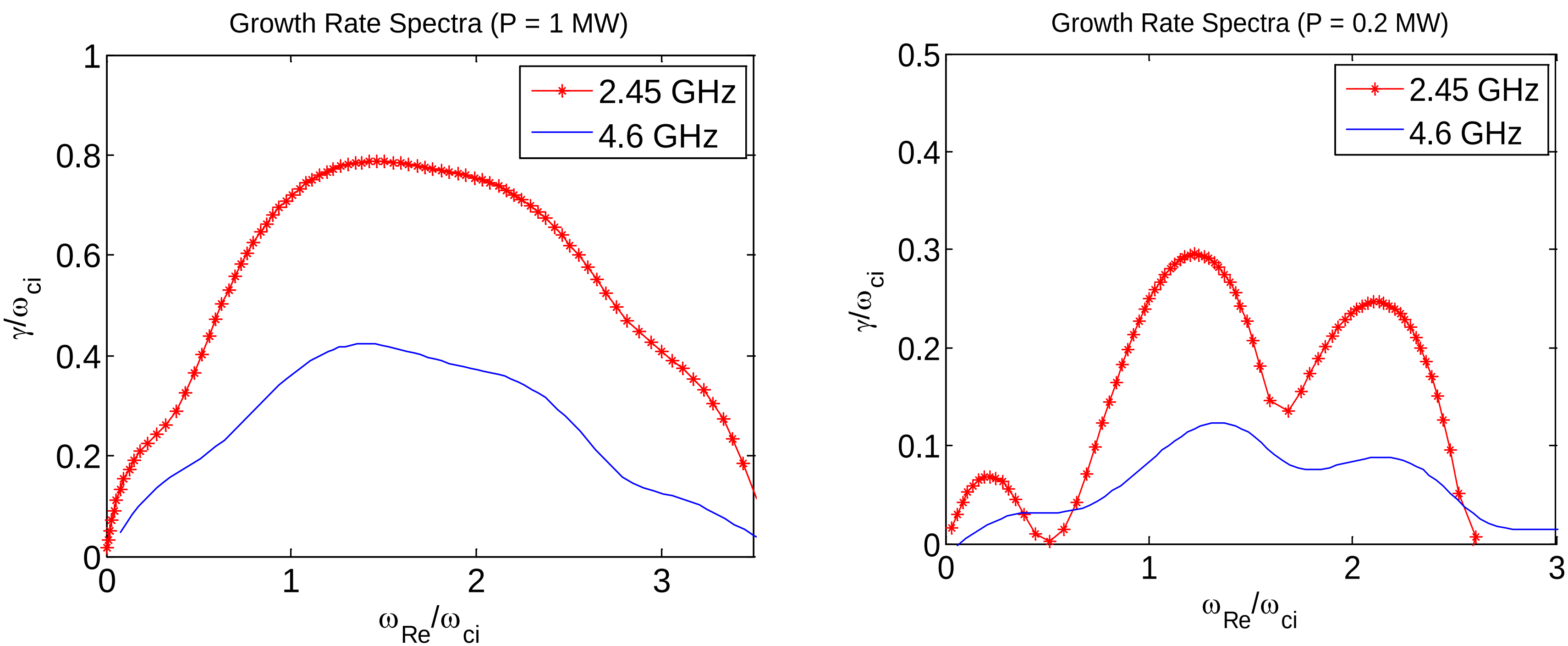

- **D plasma, n_e = 5x10^{18} m^{-3}, $T_e = T_i$ = 30 eV, B_t = 1.83 T, $n_{0//}$ = 2, and the ion mode $n_{//}$ = 7**
- **The electric field is found from the WKB approach.**

Summary

- **Converged full-wave / Fokker simulations have been obtained thus far using partially converged full-wave LH fields (N_m = 1023):**
  - **Iterated simulations with N_m = 4095 are ongoing.**
  - **Preliminary results agree qualitatively with ray tracing / Fokker Planck predictions.**
- **Development of a control level model for LHRF power deposition and CD has benefited from the use of a phenomenological model of wave scattering due to density fluctuations in order to reduce model sensitivity.**
- **Higher LH source frequency in EAST (4.6 GHz) is effective for mitigating the effects of PDI.**

Work supported by the US DOE under Contract Nos. DE-SC0010492 and DE-SC0018090.

References and Acknowledgements

[1] J. C. Wright et al, Physics of Plasmas 16, 072502 (2009).

[2] C. Yang et al, Plasma Physics and Controlled Fusion 56 125003 (2014).

[3] A. P. Smirnov and R. W. Harvey, "Calculations of the current drive in DIII-D with the GENRAY ray tracing code", Bull. Am. Phys. Soc. 40, 1837 (1995).

[4] R. W. Harvey and M. G. McCoy, "The CQL3D Fokker-Planck Code", in Proceedings of the IAEA Technical Committee Meeting on Advances in Simulation and Modeling of Thermonuclear Plasmas, Montreal, 1992, p. 527, IAEA, Vienna (1993).

[5] J. P. Lee and J. C. Wright, Computer Physics Communications 185, 2598 (2014).

PSFC
MIT Plasma Science & Fusion Center

Disruption prediction development on EAST, and proposed runaway electron research on EAST and J-TEXT

R.S. Granetz, C. Rea, R.A. Tinguely, K. Montes

MIT Plasma Science and Fusion Center, Cambridge, MA, US

D.L. Chen, B. Shen, L. Zeng

Institute of Plasma Physics, Chinese Academy of Sciences, Hefei, China

Z.Y. Chen

Huazhong University of Science and Technology, Wuhan , China

9^{th} US-China collaboration workshop

Xi’an, China

2018/06/05-07

Our disruption research on EAST is focused on two principal goals:

- Development of real time disruption prediction
  - Construction of a large database of disruption-relevant plasma parameters for training prediction algorithms (nearly finished)
  - Testing of several different machine learning methods offline to develop a credible disruption prediction algorithm
  - Incorporate algorithm into the EAST plasma control system to enable real time prediction
- Comparison of disruption prediction on EAST with similar efforts on Alcator C-Mod and DIII-D (and soon KSTAR)
  - Is a universal disruption predictor possible?
  - IAEA presentation on this in October

The EAST disruption warning database is one of several that we have developed

MIT Plasma Science & Fusion Center

Machine	Shots	Time slices (records)
C-MOD	5507	498925
EAST	14713	1209217
DIII-D	10258	2356519
KSTAR	4219	773083

~50 plasma parameters are recorded at each time slice

shot (primary key)
time (primary key)
time_until_disrupt
ip
Ip_error
dip_dt
dIpprog_dt
v_loop
p_rad
p_oh

p_icrf
p_lh
p_nbi
rad_input_frac
rad_loss_frac
n_equal_1_mode
pressure_peaking
zcur
z_error
v_z
z_times_v_z

V_0
v_mid
v_edge
beta_n
beta_p
dbetap_dt
kappa
li
dli_dt
dWmhd_dt

H98
n_e
dn_dt
r_dd
q95
q0
qstar
lower_gap
upper_gap
power_supply_railed

Greenwald_fraction
Te_width
Intentional_disruption
.
.
.
.

For *every* EAST plasma discharge, disruptive ***and*** non-disruptive, we take time slice data every 100 ms

~50 signals

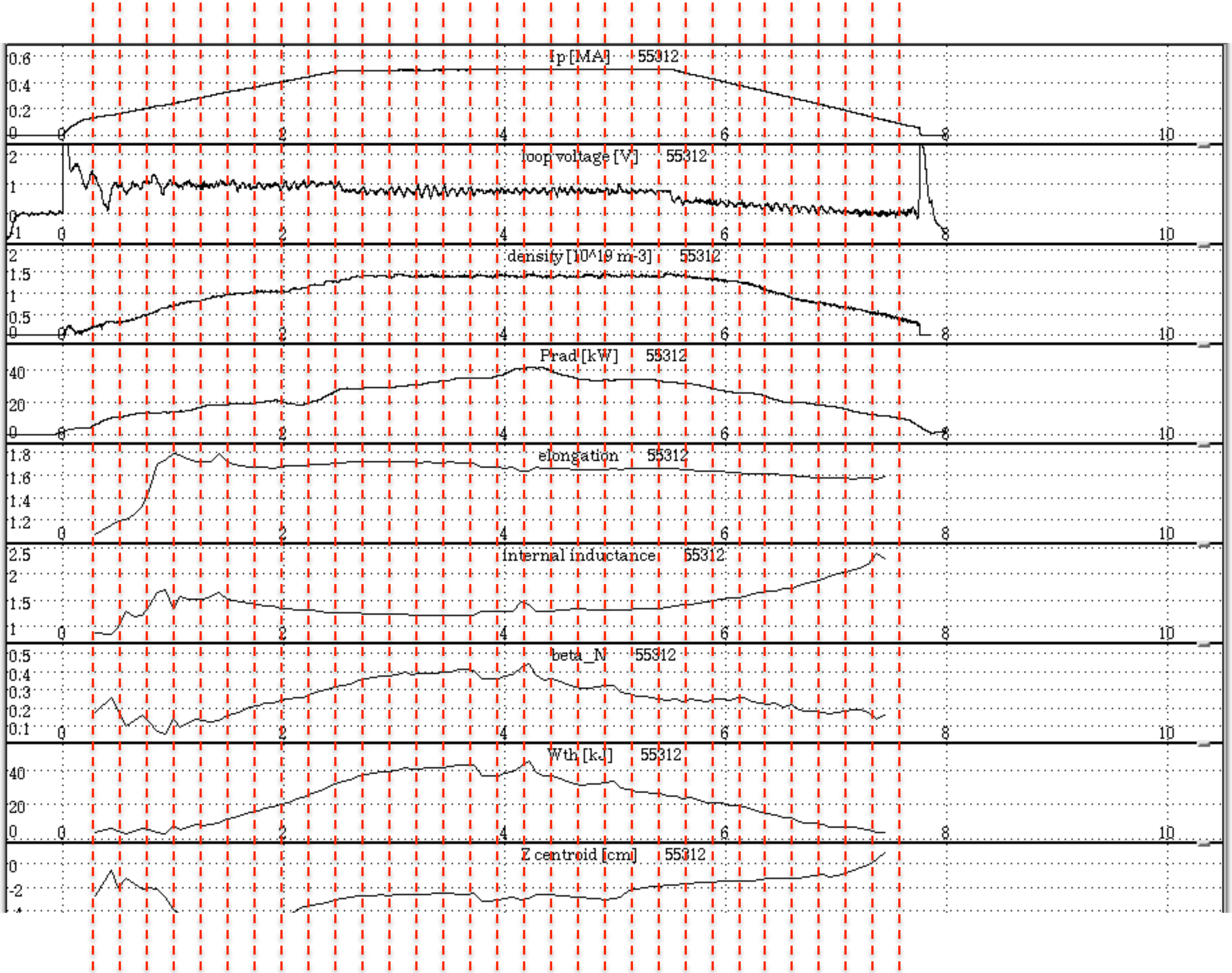

For each disruptive shot, we take *additional* time slices every 10 ms during the 250 ms period before the disruption

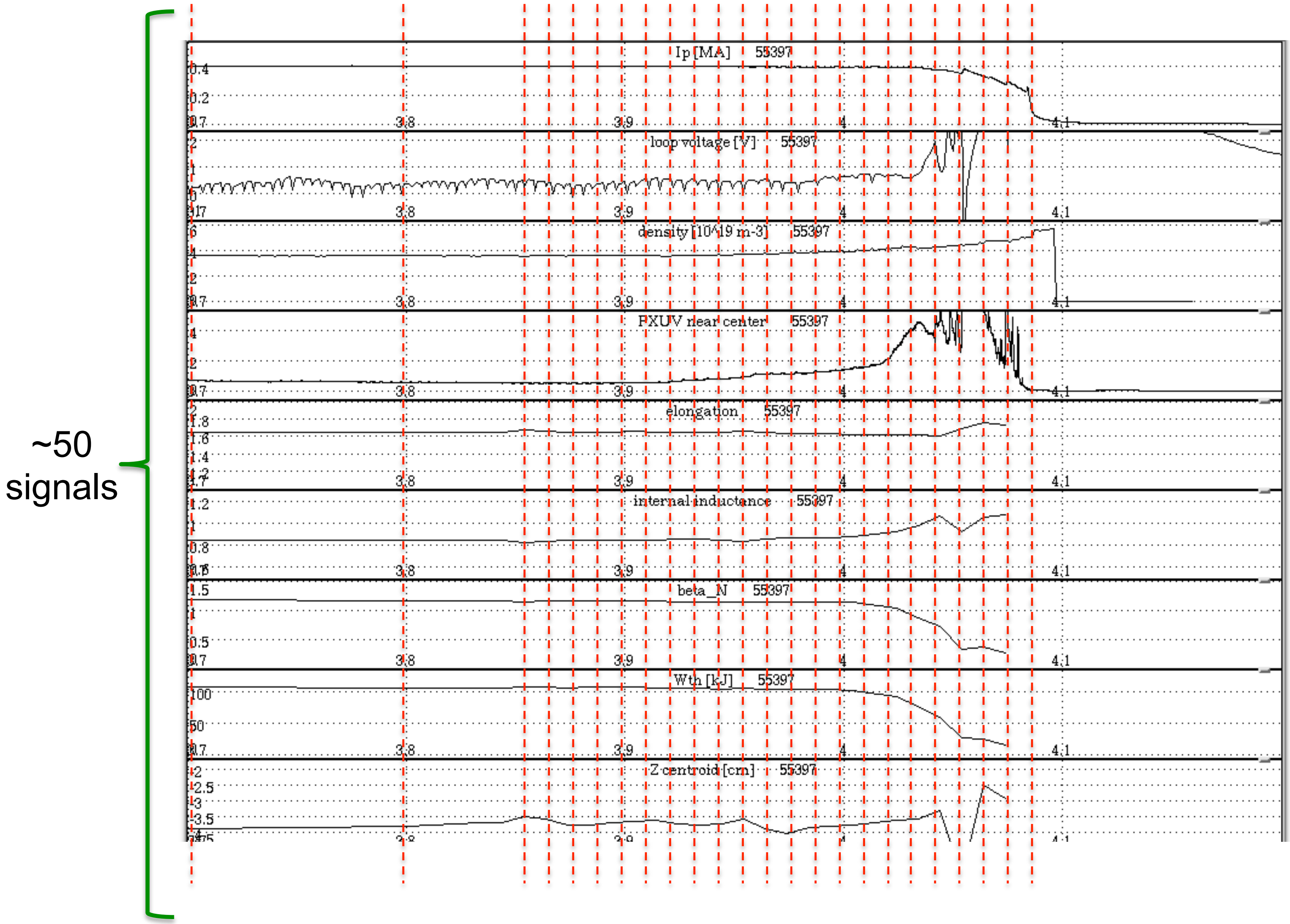

We train our prediction algorithms on a subset of the signals in the databases

MIT Plasma Science & Fusion Center

By examining the many signals in our databases we have identified a subset of 10 signals that show a clear change in behavior on *some* disruptions on *some* machines:

Signal description	Variable name
Percent error between measured and programmed plasma current, $(I_p - I_{prog})/I_p$	ip_error_frac
Poloidal beta, β_p	betap
Greenwald density fraction, n/n_G	n/nG
Safety factor at 95% of minor radius, q_{95}	q95
Normalized internal inductance, ℓ_i	li
Radiated power fraction, P_{rad}/P_{input}	prad_frac
Loop voltage, V_{loop} [V]	Vloop
Stored plasma energy, W_{th} [J]	Wmhd
$n = 1$ mode amplitude, normalized to $B_{\rm tor}$	n_equal_1_normalized
Electron temperature profile width, normalized to plasma minor radius - not available for C-Mod -	Te_width_normalized

We use this subset to train and test our machine learning algorithms

Disruption precursor behavior is very different on C-Mod, DIII-D, and EAST

MIT Plasma Science & Fusion Center

DIII-D: ℓ_i starts to increase ~400 ms before a disruption occurs on a significant fraction of disruptions.

EAST: ℓ_i shows almost no change in behavior before a disruption occurs.

C-Mod: ℓ_i starts to *decrease*, but only ~4 ms before a disruption occurs.

ℓ_i leading up to disruption time

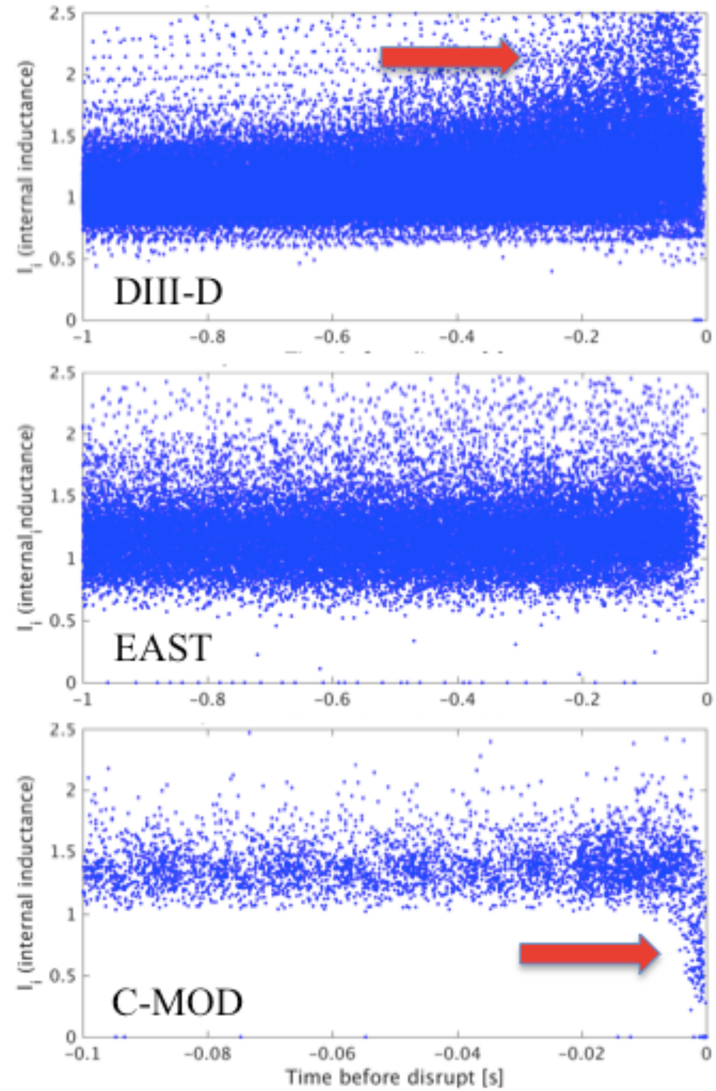

Some basic concepts of our application of AI machine learning to disruption prediction

MIT Plasma Science & Fusion Center

- We are formulating our application as a **supervised classification** problem, specifically a **binary classification** problem
  - Every time slice in the database is known a priori to belong to one of only two possible ‘classes’
  - We choose our two classes to be *‘close to disrupt’* and *‘not close to disrupt or belongs to a non-disruptive discharge’*
- Our large dataset is randomly split into a ‘training’ dataset and a ‘test’ dataset
  - An algorithm is trained (i.e. optimized) using only the data in the training set
  - The test data is then fed to the trained algorithm, and its predicted classes are compared to the a priori known classes for the test data

Most of our effort has focused on an AI Machine Learning method known as Random Forests

Random Forests consist of many independent, uncorrelated decision trees

- Each decision tree tries to divide up the space of plasma physics time slice data into the specified classes, based on objective splitting rules.

There are a number of reasons why Random Forests is an attractive Machine Learning method:

- The architecture of a Random Forest involves only one design parameter, which is easily optimized
- Different features (plasma parameters), with vastly different numerical ranges, present no issues
- For Random Forests, the degree to which each feature contributes to the classification decision can be characterized (“white box”)

The Random Forests method is easy to understand, but I don’t have the 15 minutes that it takes to explain them

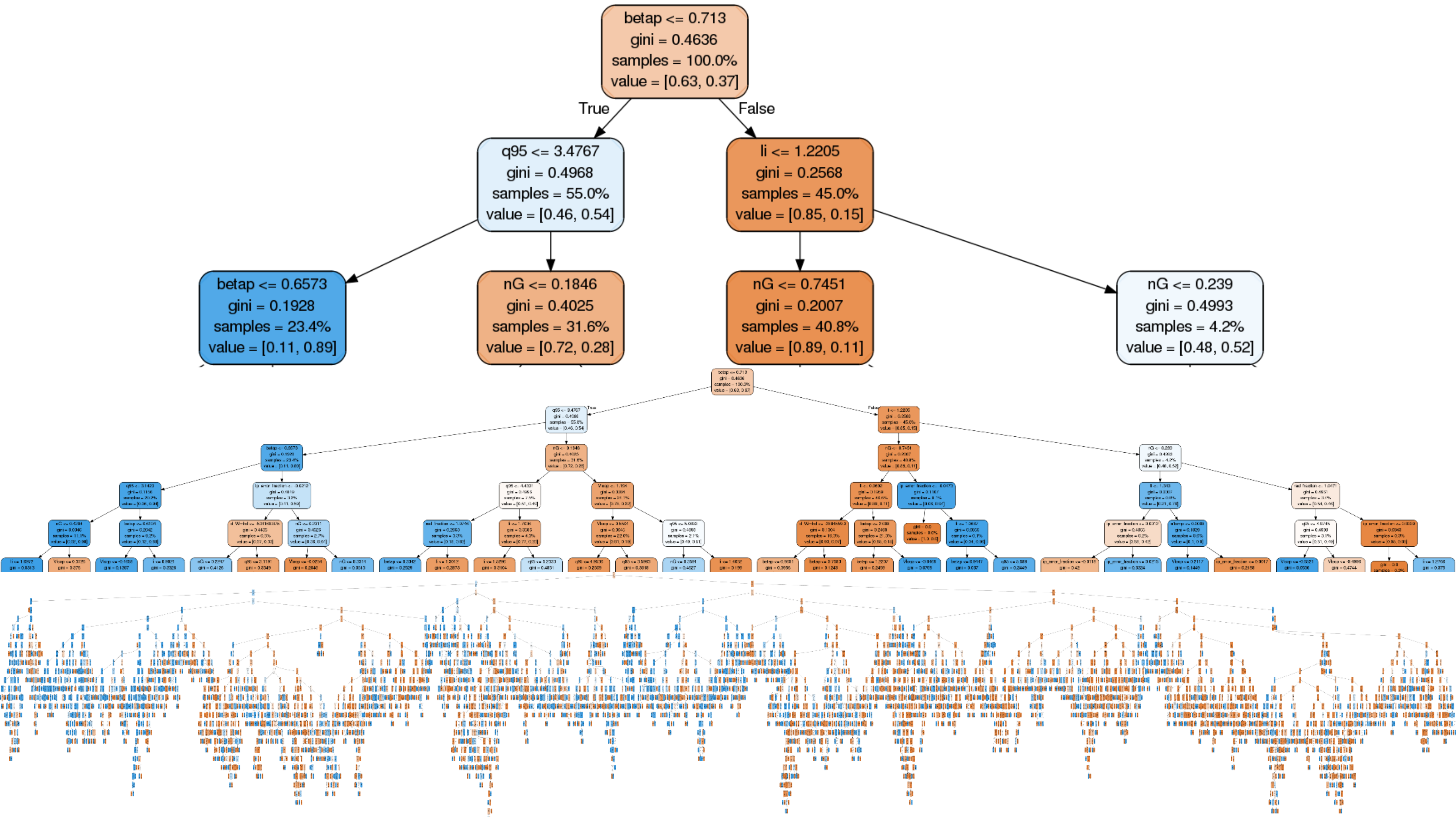

Comparison of Random Forest performance on DIII-D, EAST, and C-Mod

MIT Plasma Science & Fusion Center

Results are for flattop period only, for all shots in 2015 campaigns

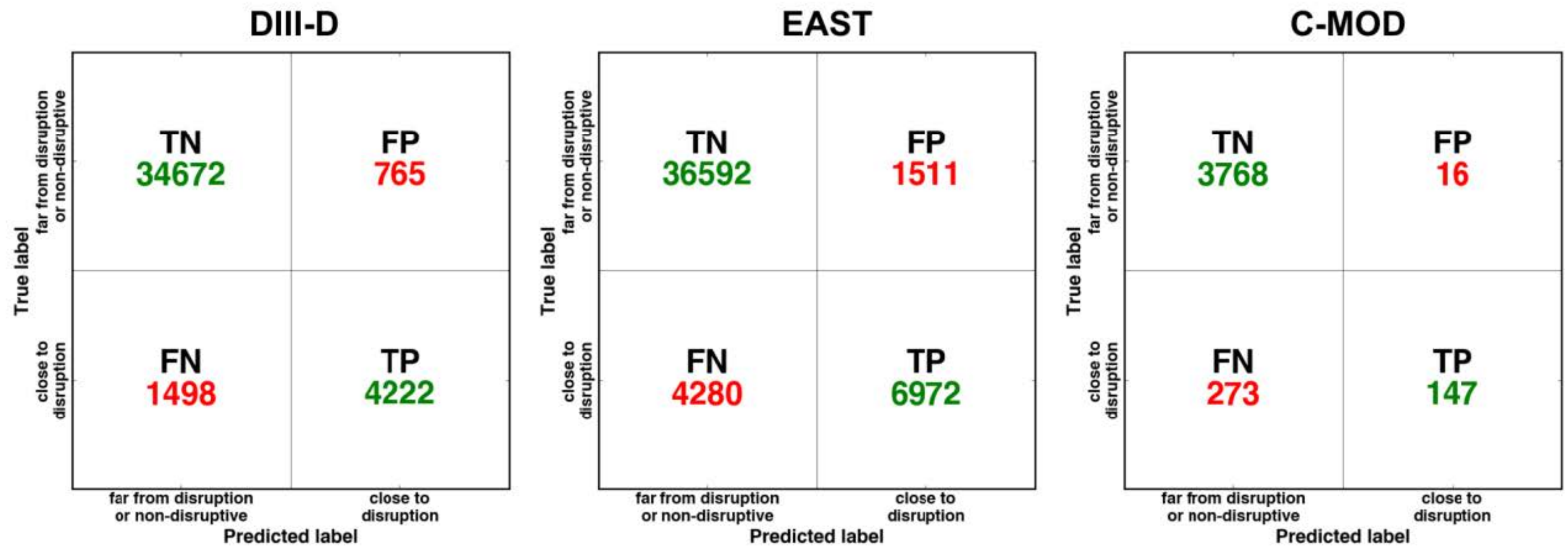

"recall" = TP/(TP+FN) = fraction of "close to disrupt" that are correctly predicted

DIII-D	EAST	C-MOD
73.8%	62.0%	35.0%

Miss rate = 1 - recall = "close to disrupt" that are not caught

False alarm fraction = FP/(TP+FP)

"F1 score" = weighted combination of miss rate and false alarm rate

But Random Forests lack one significant feature which may be important for disruption prediction

RF classification is done on each time slice independently

- Information from previous classification decisions is not used in determining the classification of the current time slice
- The classification of the current time slice is not available for classification decisions of future time slices.

Neural Networks are another AI method for classification problems

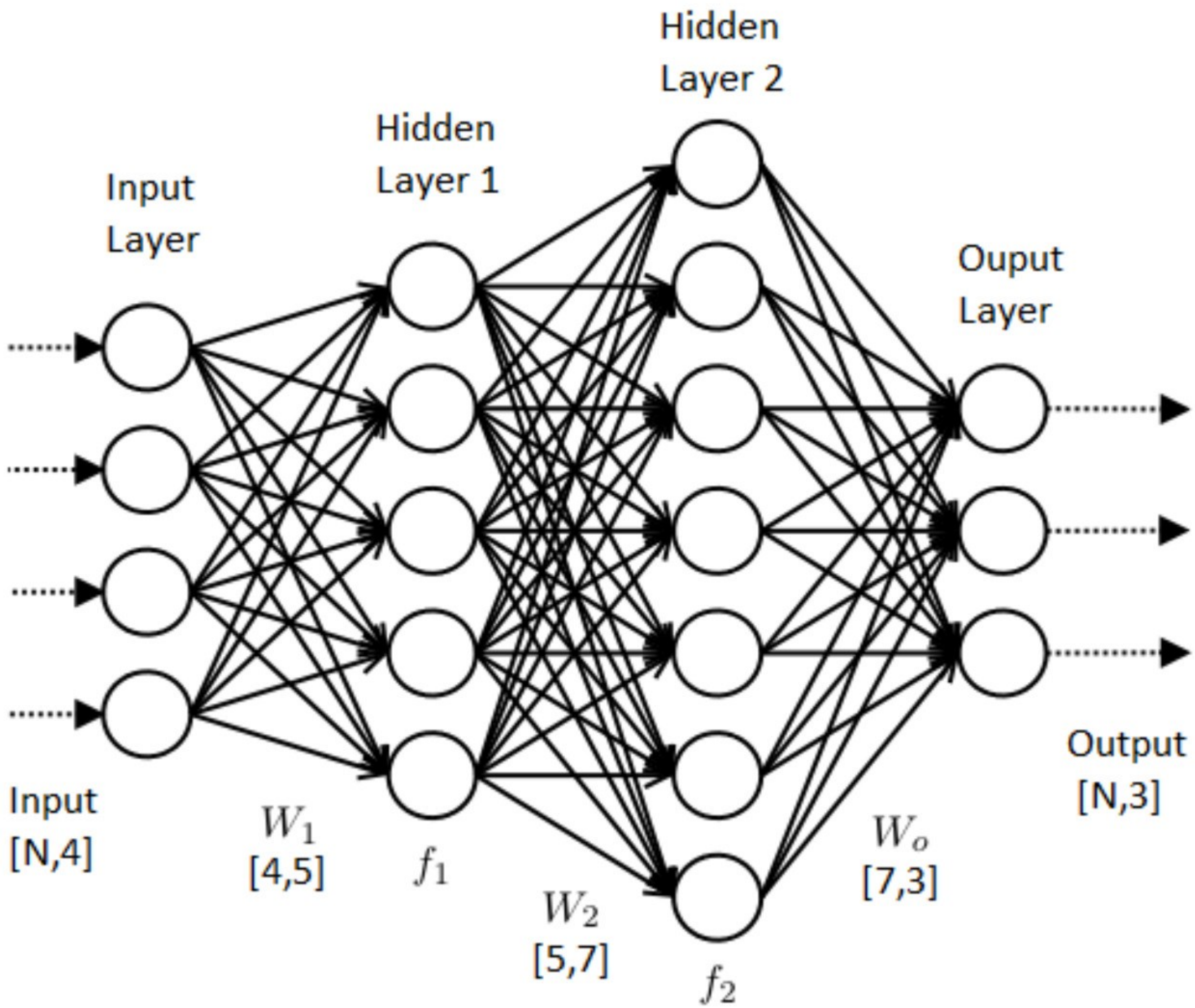

Neural Networks are another AI method for classification problems

Many design parameters that can be difficult to determine:

- How many hidden layers?
- How many nodes in each hidden layer?
- 1000’s or millions of weights to determine/optimize
  - Deep Learning; back-propagation;
- Difficult to determine the degree to which each feature contributes to the classification decision (“black box”)

But their complexity can incorporate features such as temporal history

Recurrent Neural Networks (RNN's) have the capability to include past classification information in current and future decisions

LSTM Layer Architecture

This diagram illustrates the flow of a time series *X* with *D* features of length *S* through an LSTM layer. In this diagram, *h* denotes the output (also known as the *hidden state*) and *c* denotes the *cell state*.

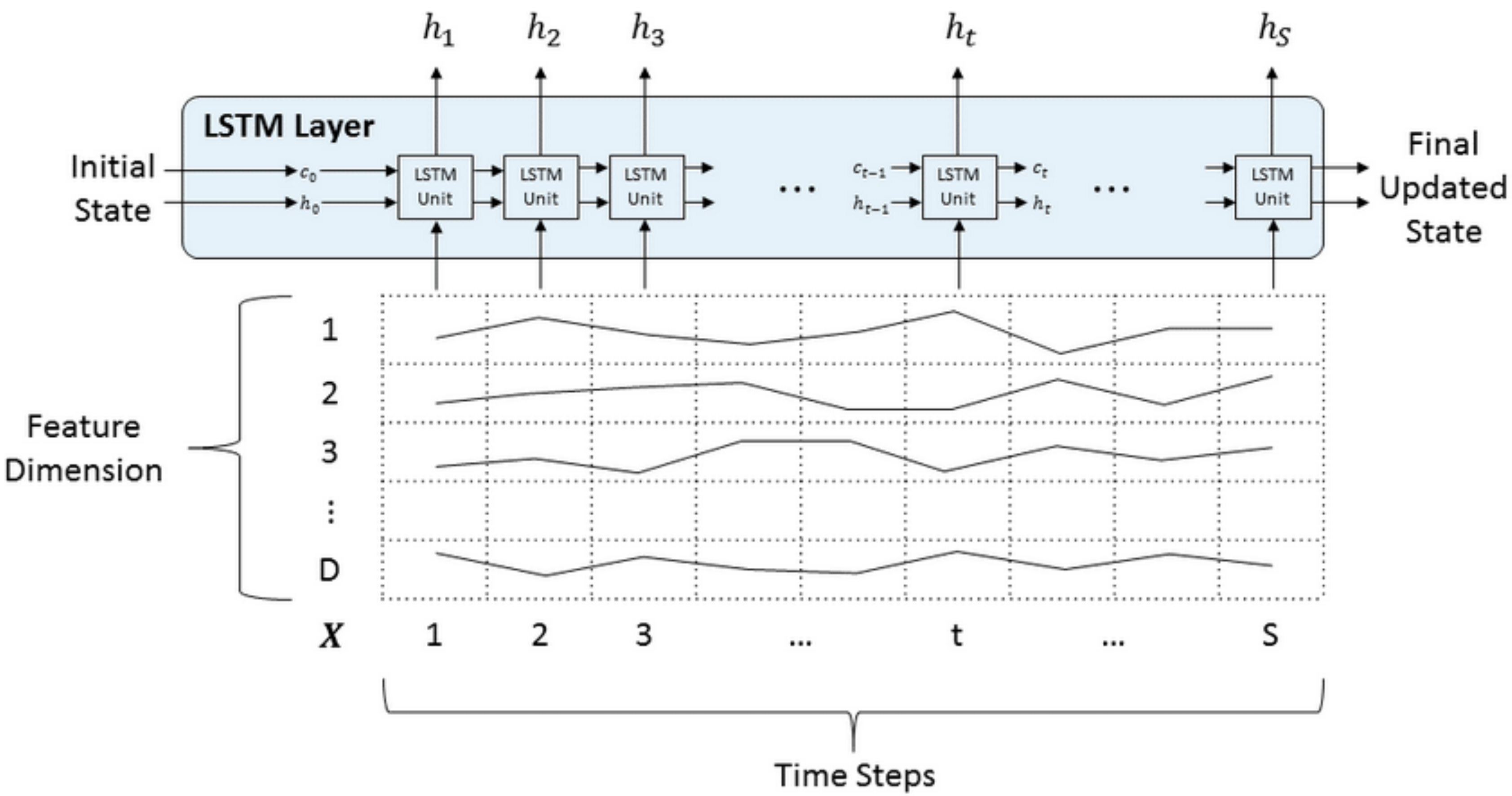

Recurrent Neural Networks (RNN's) have the capability to include past classification information in current and future decisions

Component	Purpose
Input gate (i)	Control level of cell state update
Forget gate (f)	Control level of cell state reset (forget)
Layer input (g)	Add information to cell state
Output gate (o)	Control level of cell state added to output state

This diagram illustrates the flow of data at time step t. The diagram highlights how the gates forget, update, and output the cell and output states.

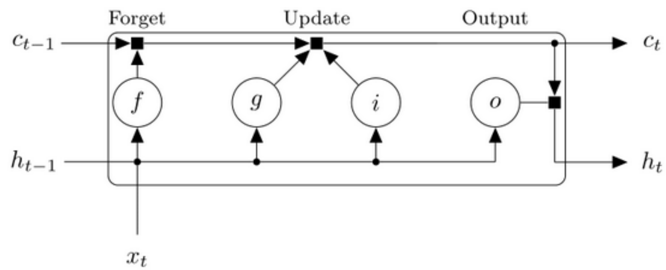

The learnable weights of an LSTM layer are the input weights W (InputWeights), the recurrent weights R (RecurrentWeights), and the bias b (Bias). The matrices W, R, and b are concatenations of the input weights, the recurrent weights, and the bias of each component, respectively. These matrices are concatenated as follows:

$$W = \begin{bmatrix} W_i \\ W_f \\ W_g \\ W_o \end{bmatrix}, R = \begin{bmatrix} R_i \\ R_f \\ R_g \\ R_o \end{bmatrix}, b = \begin{bmatrix} b_i \\ b_f \\ b_g \\ b_o \end{bmatrix},$$

where i, f, g, and o denote the input gate, forget gate, layer input, and output gate, respectively.

The cell state at time step t is given by

$$c_t = f_t \odot c_{t-1} + i_t \odot g_t,$$

where $\odot$ denotes the Hadamard product (element-wise multiplication of vectors).

The output (hidden) state at time step t is given by

$$h_t = o_t \odot \tanh(c_t).$$

This table shows the formula for each component at time step t.

Component	Formula
Input gate	$i_t = \sigma(W_i x_t + R_i h_{t-1} + b_i)$
Forget gate	$f_t = \sigma(W_f x_t + R_f h_{t-1} + b_f)$
Layer input	$g_t = \tanh(W_g x_t + R_g h_{t-1} + b_g)$
Output gate	$o_t = \sigma(W_o x_t + R_o h_{t-1} + b_o)$

Here, σ denotes the sigmoid function given by $\sigma(x) = (1+e^{-x})^{-1}$.

We have very recently started to train a simple, one-hidden-layer RNN on EAST disruption data

MIT Plasma Science & Fusion Center

```
fraction of disruptive time slices in training dataset =  9.54%
fraction of disruptive time slices in test dataset =  9.33%

layers =
  5x1 Layer array with layers:

     1   ''   Sequence Input          Sequence input with 9 dimensions
     2   ''   LSTM                    LSTM with 50 hidden units
     3   ''   Fully Connected         2 fully connected layer
     4   ''   Softmax                 softmax
     5   ''   Classification Output   crossentropyex
Training on single CPU.
|==========================================================================================|
|     Epoch     |   Iteration   | Time Elapsed |  Mini-batch  |  Mini-batch  | Base Learning|
|               |               |  (seconds)   |     Loss     |   Accuracy   |     Rate     |
|==========================================================================================|
|             1 |             1 |         0.05 |       0.3987 |       68.87% |       0.0100 |
|             1 |            50 |         3.76 |       0.1472 |       94.56% |       0.0100 |
|             1 |           100 |         6.85 |       0.0870 |       97.22% |       0.0100 |
|             1 |           150 |        10.53 |       0.1010 |       96.50% |       0.0100 |
|             1 |           200 |        14.38 |       0.1002 |       96.64% |       0.0100 |
|             1 |           250 |        18.74 |       0.1439 |       95.08% |       0.0100 |
|             2 |           300 |        22.99 |       0.1460 |       93.68% |       0.0100 |
|             2 |           350 |        26.66 |       0.0641 |       97.69% |       0.0100 |
|             2 |           400 |        31.03 |       0.0865 |       96.86% |       0.0100 |
|             2 |           450 |        35.41 |       0.1296 |       97.51% |       0.0100 |
|             2 |           500 |        40.00 |       0.1130 |       97.56% |       0.0100 |
|             2 |           504 |        40.46 |       0.0540 |       98.14% |       0.0100 |
|==========================================================================================|

disrupt_class_threshold_time = 1.000 s

TP = 3644  FP = 1354  TN = 85546  FN = 5294

 accuracy  precision  recall    F1
  0.933      0.723    0.480   0.577
```

We have very recently started to train a simple, one-hidden-layer RNN on EAST disruption data

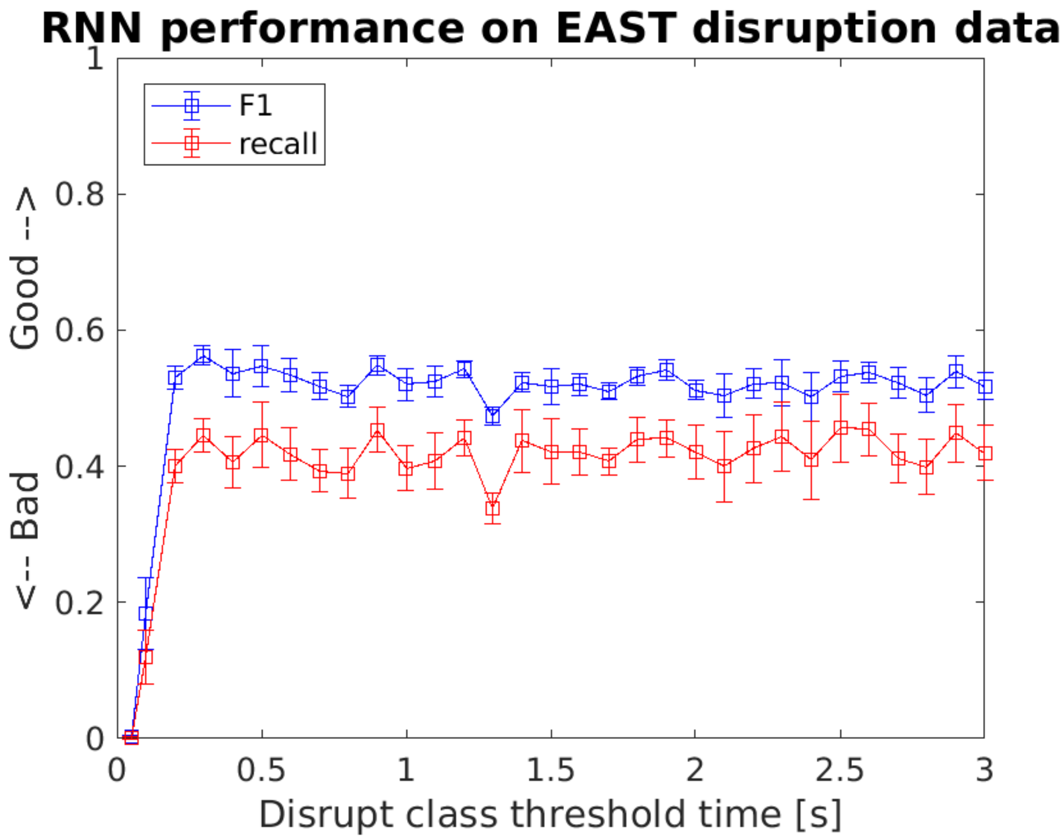

Future plans for disruption prediction work

MIT Plasma Science & Fusion Center

- Continue work on database
  - Add 2018 data; normalizations; add real time signals, etc.
- Optimize recurrent neural network
  - # of hidden layes, # of nodes per layer, …
- Install in plasma control system
  - Algorithm must be trained on actual signals coming into the PCS, including EFIT RT
  - Algorithm must be packaged in a way that can be incorporated into PCS, and receive/pass data with to/from PCS
  - Our recent experience installing a disruption predictor into the DIII-D PCS should help a lot with EAST

Examples of our real time disruption predictor operating in the DIII-D PCS

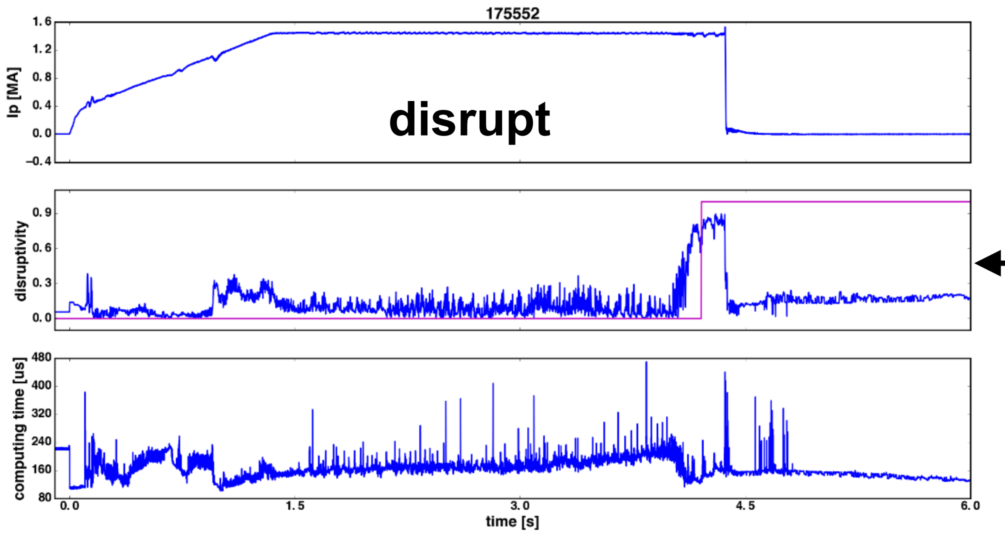

output begins climbing ~350 ms before the disruption occurs

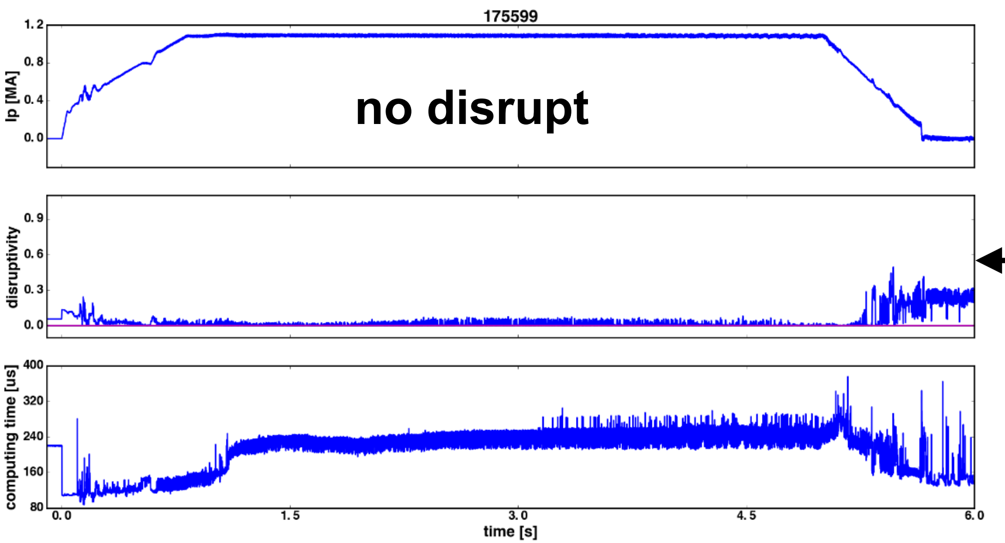

no warning alarm is triggered in healthy plasma

Continue with disruption mitigation on EAST

We also propose to collaborate with studies of runaway electrons on EAST and J-TEXT

- RE research on EAST: Zeng Long
  - IR imaging; studies of primary and avalanche growth processes
  - Zeng will visit MIT in October to discuss collaboration
- RE research on J-TEXT: Chen ZhongYong
  - IR imaging; MGI and SPI mitigation of runaways
- RE research on C-Mod
  - Synchrotron spectral analysis
    - We can bring the spectrometers to EAST and/or J-TEXT
  - Visible synchrotron imaging analysis

C-Mod RE research

Synchrotron spectra can inform energy distribution of runaway electrons (REs) [Tinguely NF 2018]

- Absolutely-calibrated visible spectrometers
- B_0 = 2.7, 5.4, 7.8 T
- Test particle model for energy [Martín-Solís PoP 1998] and density [Connor NF 1975, Rosenbluth NF 1997]
- Synthetic diagnostic SOFT [Hoppe NF 2018] generated synthetic spectra
- For fixed E/E_C, increasing B_0 is consistent with decreasing RE energy

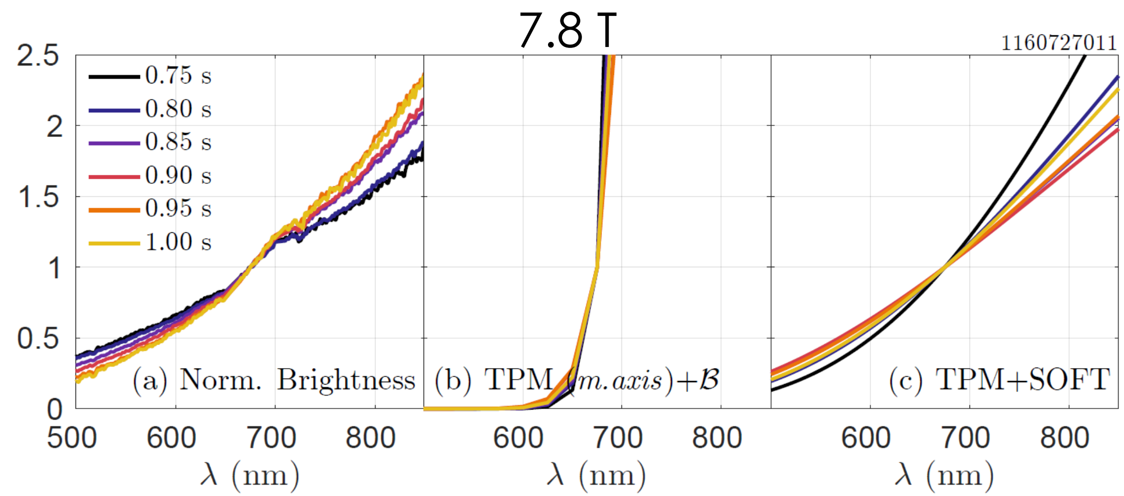

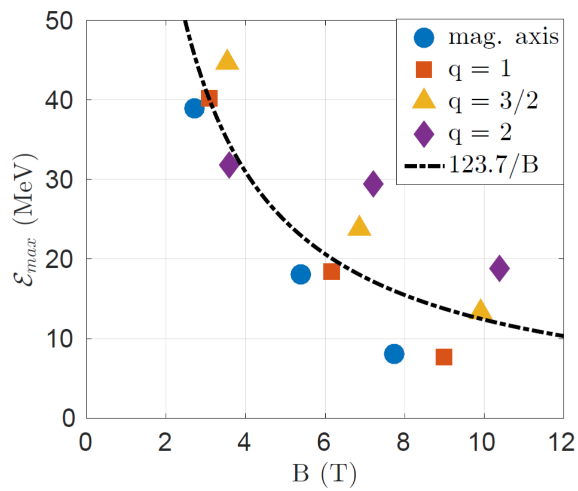

Plasma Science and Fusion Center

C-Mod RE research

Synchrotron images can inform spatial distribution of REs

- Distortion-corrected, wide-view visible camera
- Full momentum space distributions from CODE [Landreman CPC 2014] needed to capture spatial effects
- MHD activity seems to increase RE transport, shrinking size of RE beam
- Distinct periods of RE growth are seen, including secondary avalanching
- To present at Runaway Electron Meeting and EPS

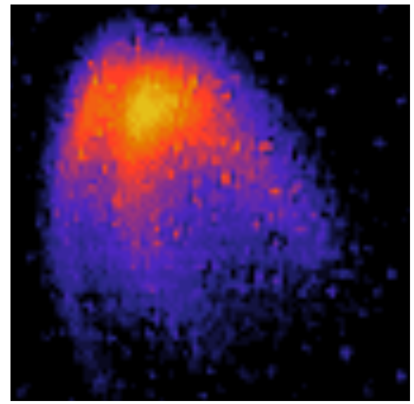

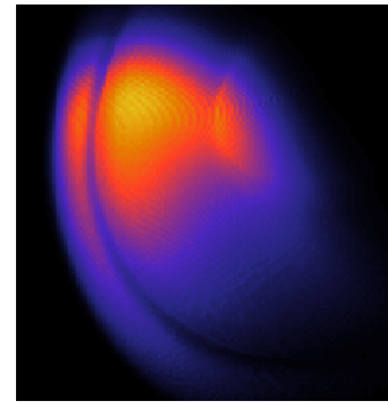

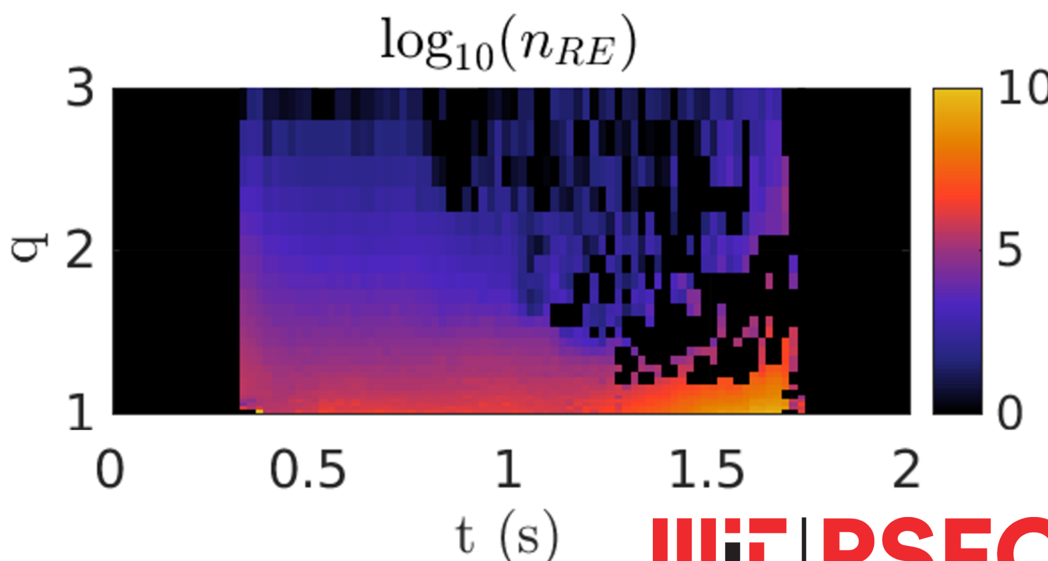

Plasma Science and Fusion Center

Development of fullwave RF simulation code based on the open source FEM library

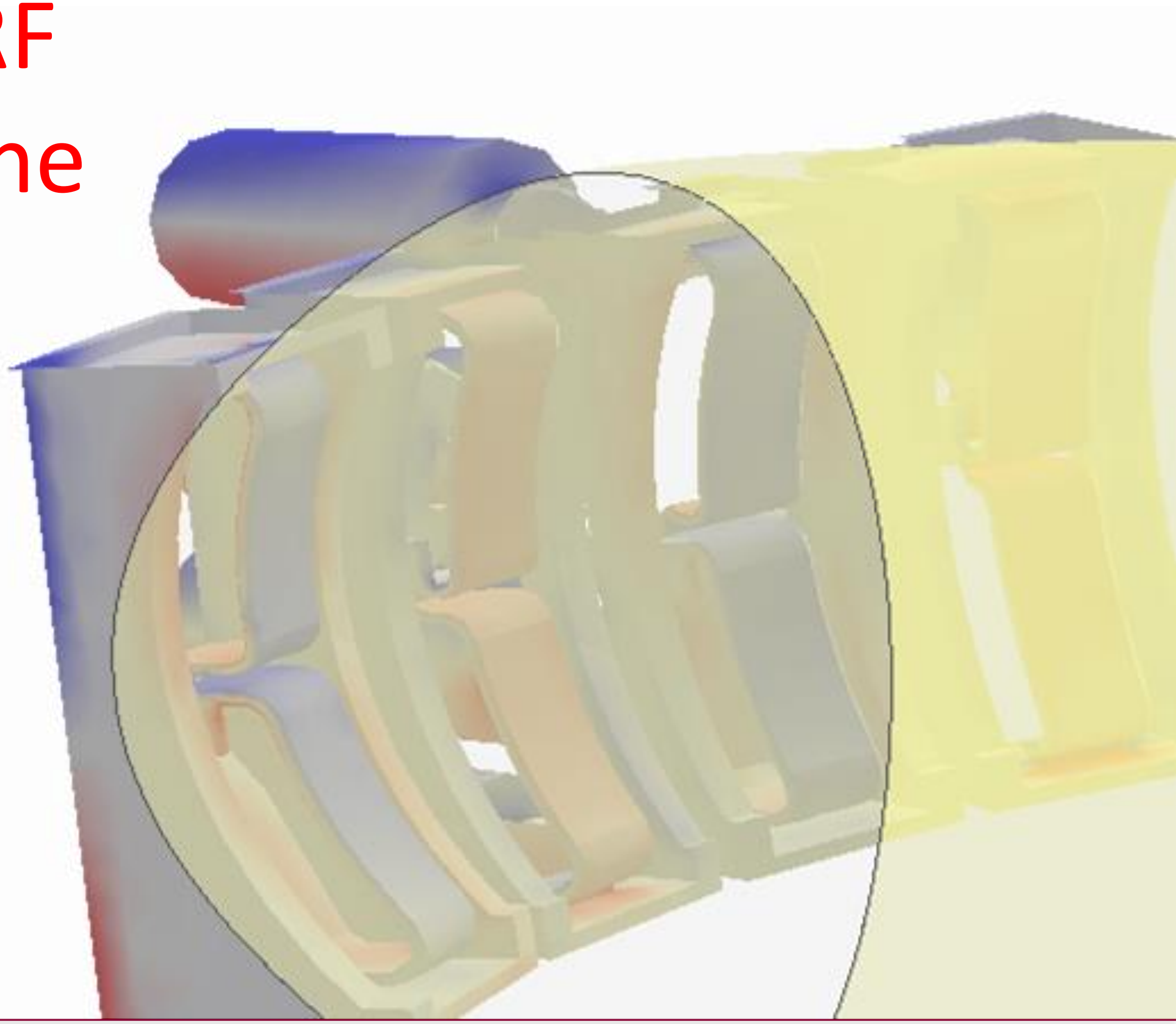

S. Shiraiwa and J. C. Wright

With contributions from

P. T. Bonoli, N.Bertelli[1], J. Myra[2], T. Kolev[3], M. Stowell[3],
Y. Lin, C. Lau[4], G. Wallace, S. Wukitch, L. Zhou, W. Beck, the Alcator C-Mod team and RF-SciDAC

PSFC-MIT, PPPL[1], Lodestar[2], LLNL[3], and ORNL[4]

Leading-class computing facilities allow for accurate RF wave physics simulations in core and edge regions with great detail

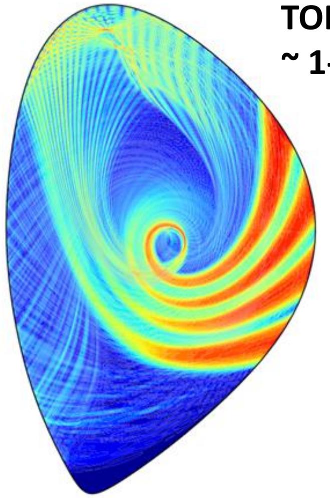

TORLH
~ 1-10k CPU Hours

AORSA 3D for ITER
~ 1 million CPU Hours

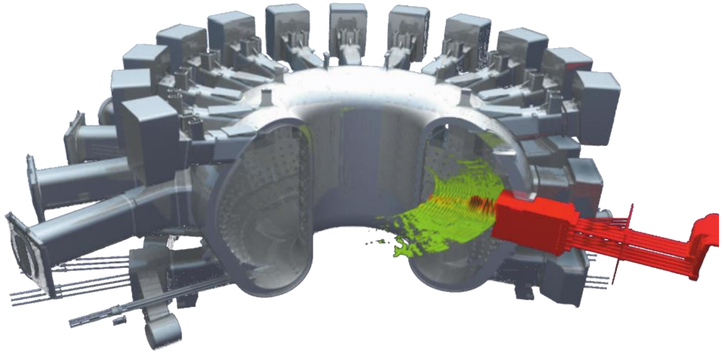

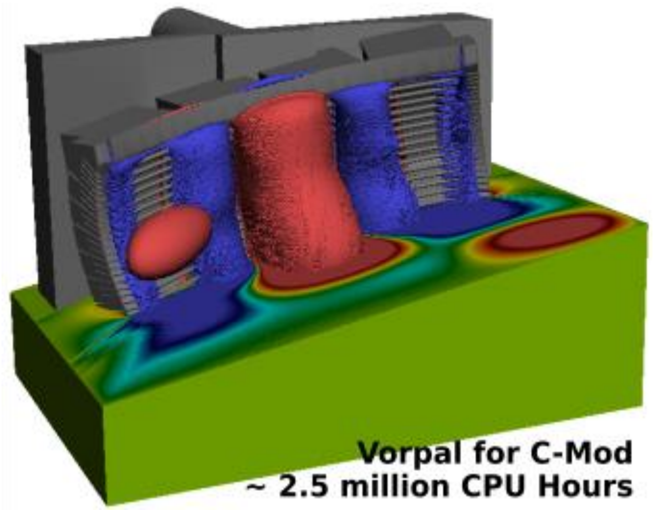

These models compute RF wave propagation and absorption including linear and non-linear effects

- Full wave spectral code simulations of core LH and IC waves
- FDTD (finite difference time domain) simulation of ICRF antenna on C-Mod

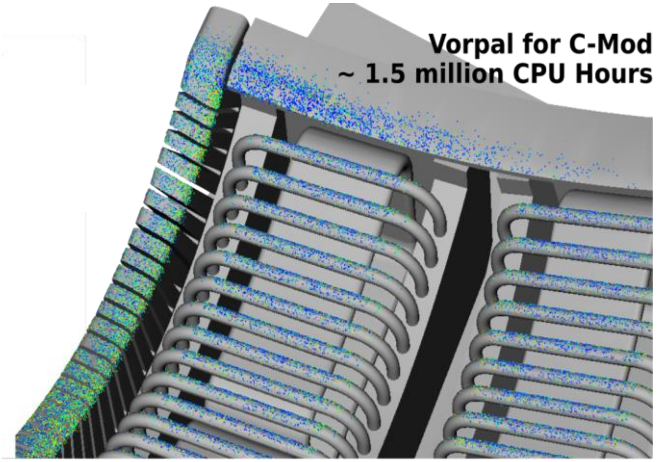

These models are now being able to couple RF non-linear effects such as modification of velocity distribution function and RF sheath rectified potential.

However, core and edge regions are modeled separately…

Requirements for self-consistent (hot core + realistic 3D antenna) RF simulations have been widely recognized

Many physics issues require to couple a hot core plasma with an edge (antenna and SOL) model having high geometrical fidelity

- Edge parasitic losses observed on many experiments (Alcator C-Mod ICRF[1]/LH[2], NSTX HHFW[3])
- Antenna coupling in 3D geometries (C-Mod field aligned ICRF, stellarators)
- Multiple-pass absorption regimes
- Impact of edge turbulence (See next talk).

- "monolithic" approach ?
  - Half torus ICRF simulation on Alcator C-Mod using a FDTD code (cold core plasma)
  - FEM (finite element method) simulation of LH waves (iterative inclusion of electron Landau damping)

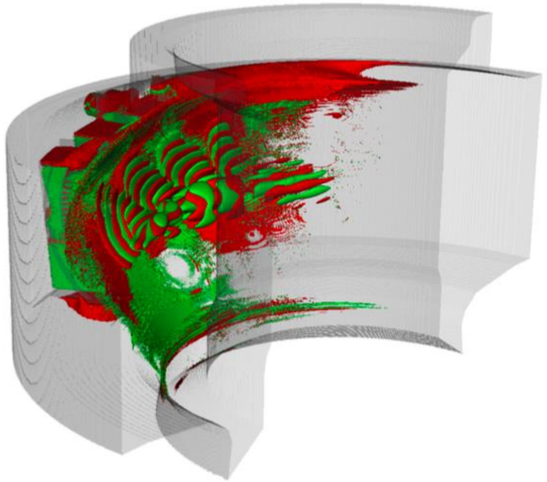

Vorpal half C-Mod ICRF simulation (FDTD)

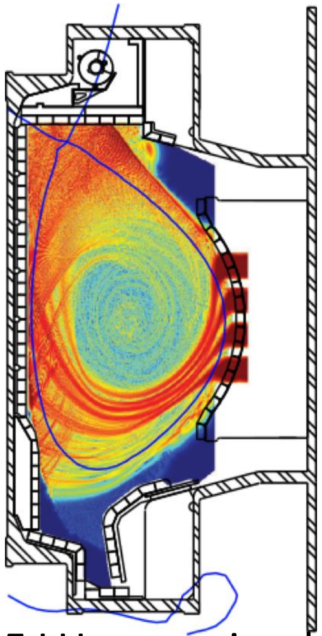

LHEAF LH wave simulation (FEM)

1) S. J. Wukitch et al, Phys. Plasmas **20**, 056117 (2013)
2) G. M. Wallace, et al., Phys. Plasmas **17**, 082502 (2010)
3) R. J. Perkins, et al., Phys. Plasmas **22**, 042506 (2015)
4) T. G. Jenkins and D. N. Smithe , 26th IAEA FEC (2016) TH/P4-34
5) O. Meneghini Ph.D Thesis (2012)

Outline

- HIS (Hybrid integration SOL) approach
  - Formulation/implementation
  - Verification using a stand alone TORIC simulation
- 2D Simulation and comparison with Alcator C-Mod experiment
- 3D Simulation
  - w/o 3D antenna structure
  - with 3D antenna structure
- Future plans and conclusion

HIS (Hybrid integration of SOL)-TORIC

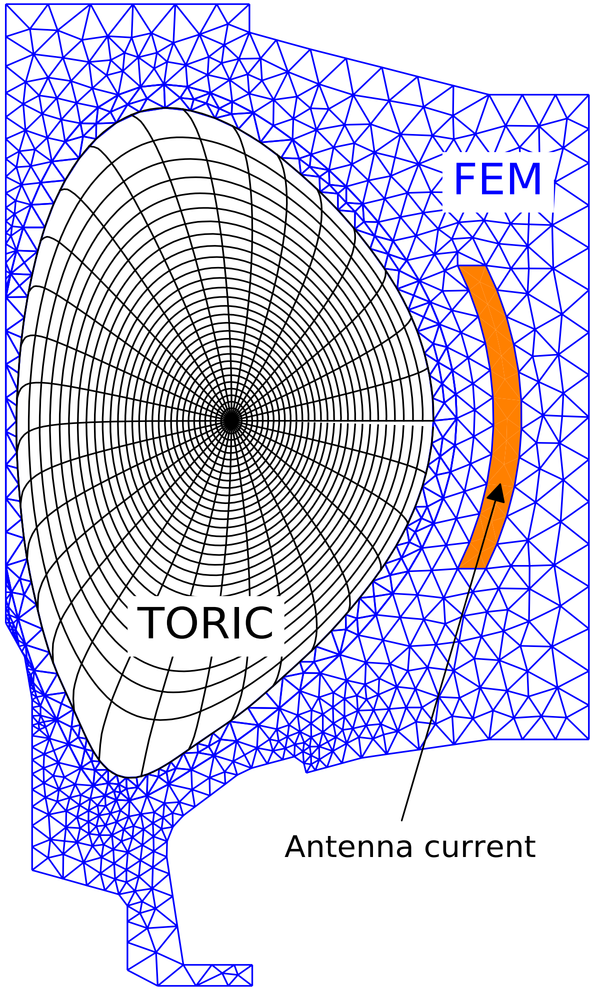

Core

- **Axisymmetric** flux surface regular grid
- Hot plasma conductivity
- Dense Matrix Solver

Edge

- **Unstructured mesh** with complicated geometry (either 2D or **3D**)
- Cold plasma with collision.

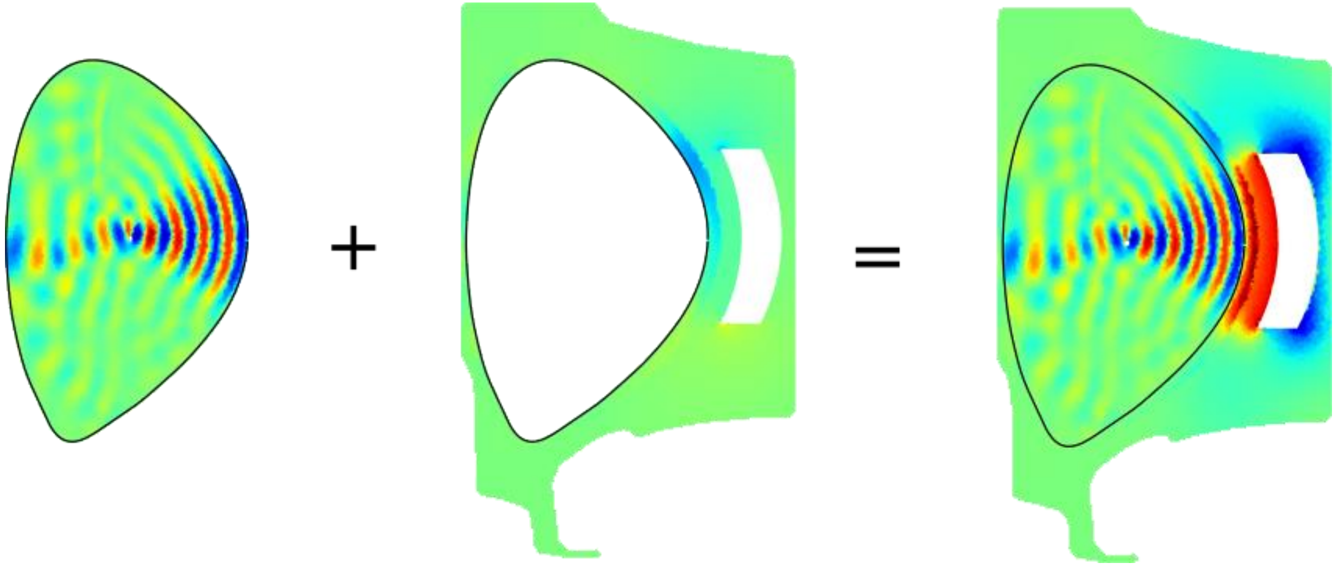

Core and edge connecting rule = cascading of RF components

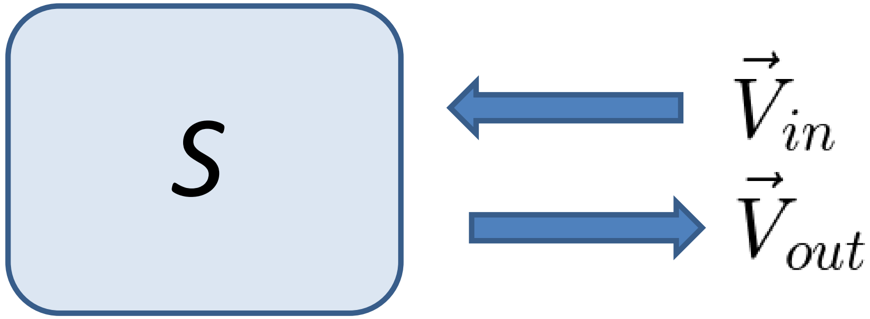

RF network characterized by the Scattering matrix, S

$$\vec{V}_{out} = S\,\vec{V}_{in}$$

When connecting two networks…

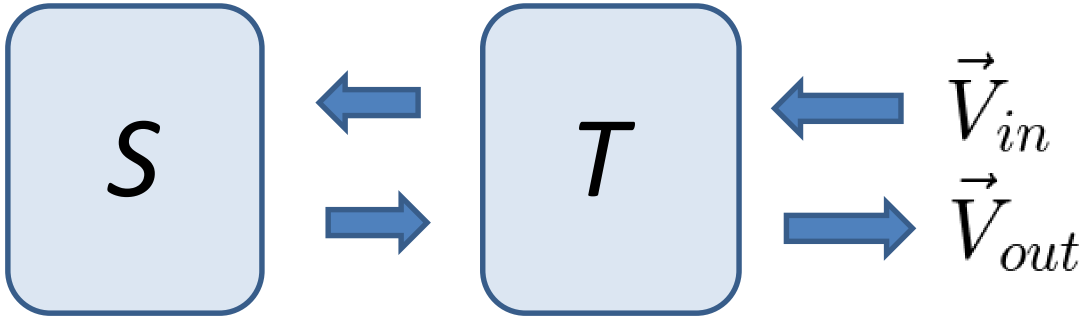

$$\vec{V}_{out} = U(T_2, S) \cdot T_1 \vec{V}_{in}$$

T_1: response to the power from the external input

T_2: response to the power from S

MIT PSFC Plasma Science and Fusion Center

Final solution constitutes from three components

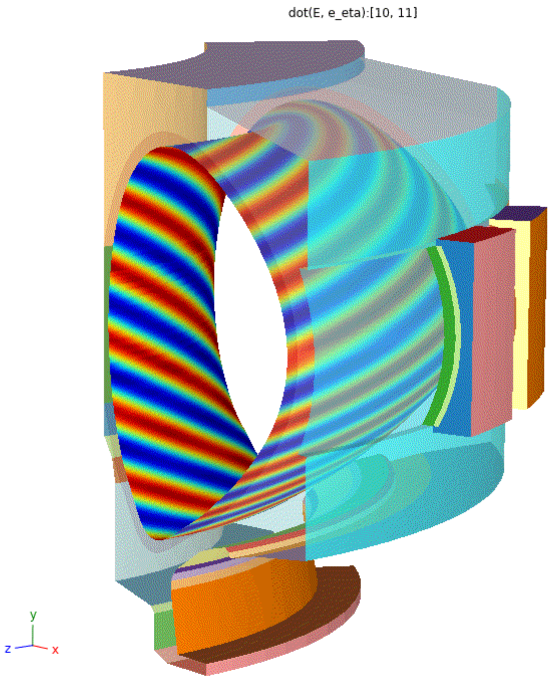

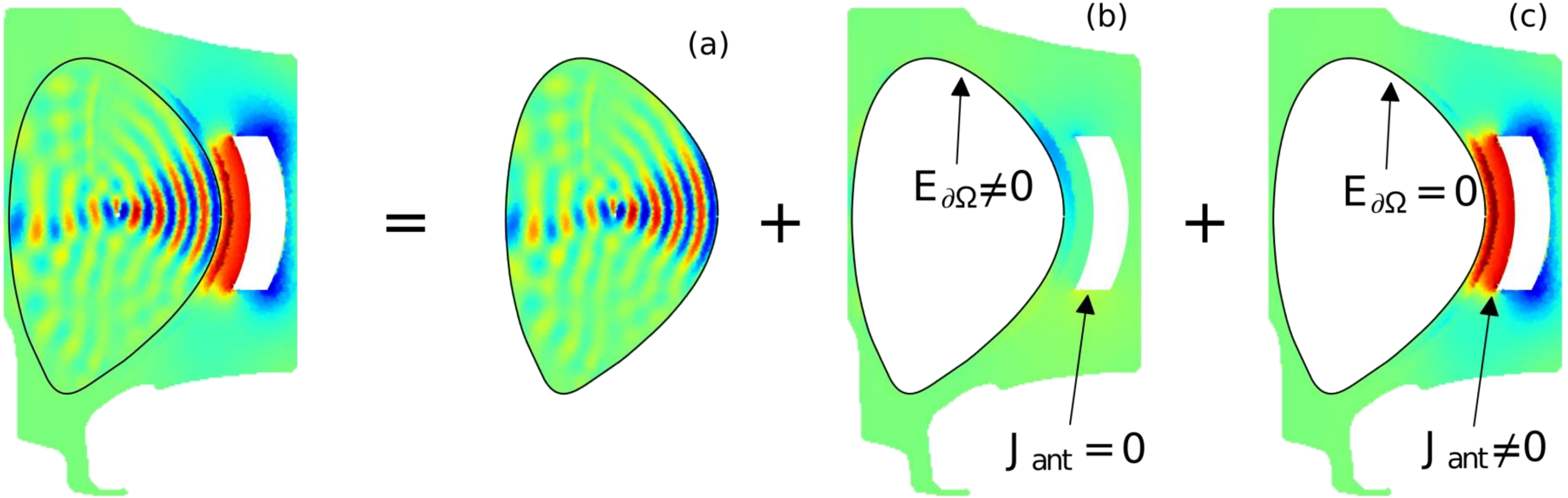

- Fourier decomposed modes (poloidal/toroidal) , not discrete RF port voltages.
- This method is exact – no approximations.
- Equivalent for requiring the continuity of tangential E and B on the connecting boundary.
- Changing antenna excitation does not require re-computing (b)

Derivation and verification using COMSOL for edge L S. Shiraiwa et. al, et al. N.F. (2017, J. Wright et. al., RF conf. (2017)

The reconstructed solution is very similar to a standalone TORIC simulation.

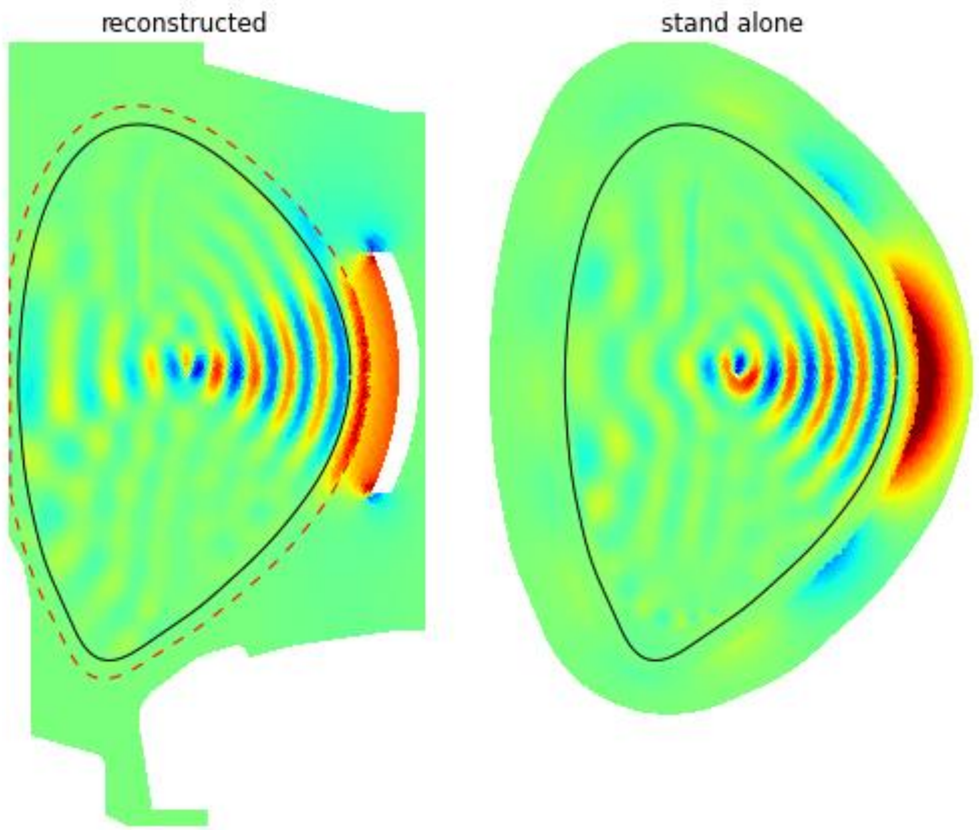

- In the core region, the superimposed solution (left) agrees well with the core solution of TORIC stand alone simulation (right) providing verification of the method.
- There is only vacuum outside LCF.

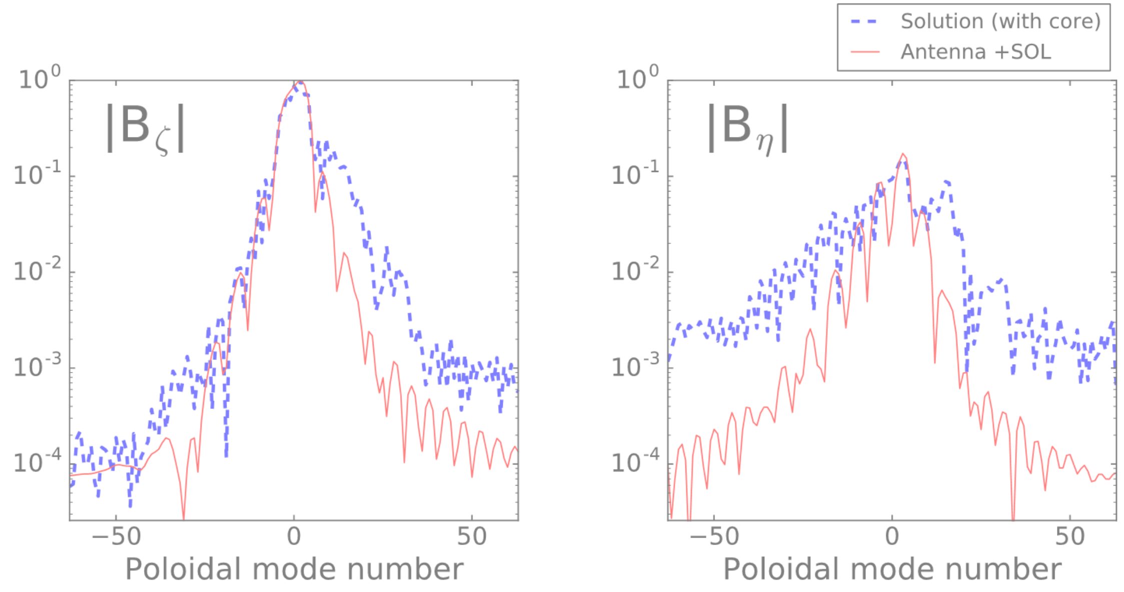

The reconstructed solution is very similar to a standalone TORIC simulation.

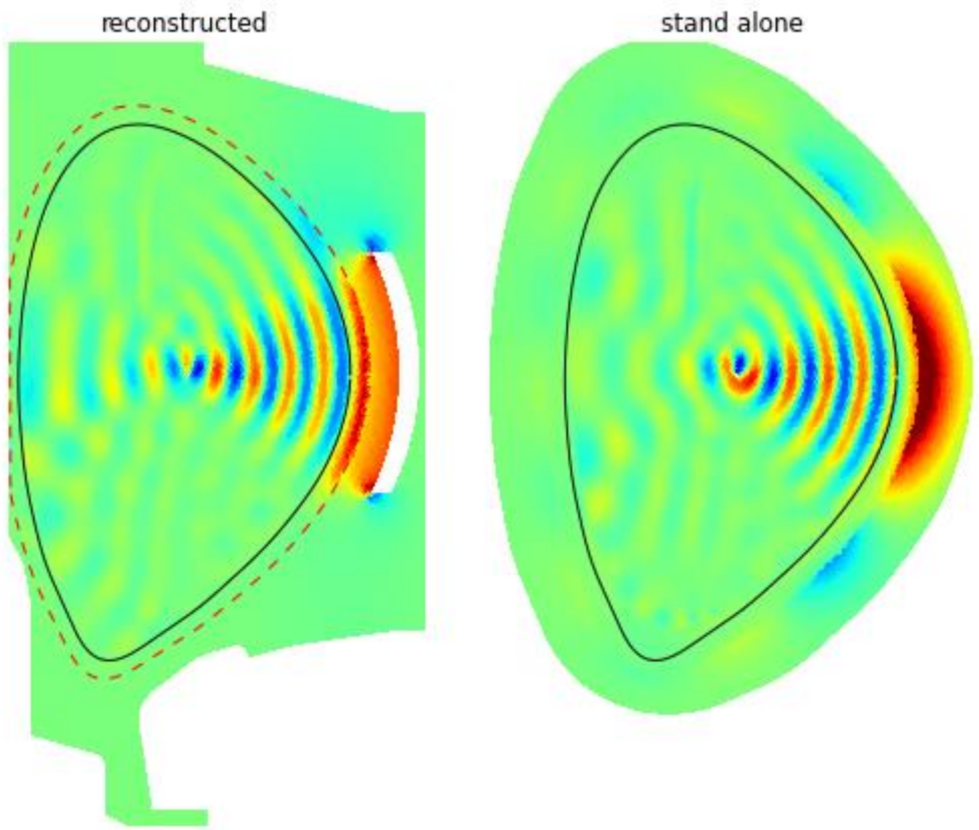

- In the core region, the superimposed solution (left) agrees well with the core solution of TORIC stand alone simulation (right) providing verification of the method.
- There is only vacuum outside LCF.
- Mode amplitude of superimposed solution (blue) spread wider than the antenna excitation amplitude (red).

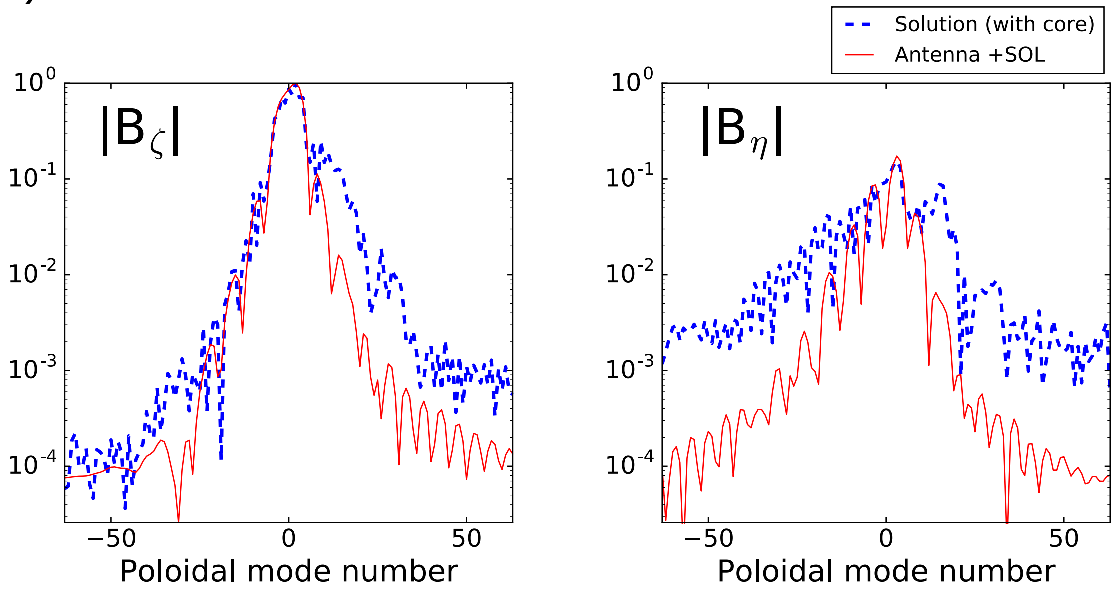

Detailed verification : E_ψ continuity is retained at domain boundary

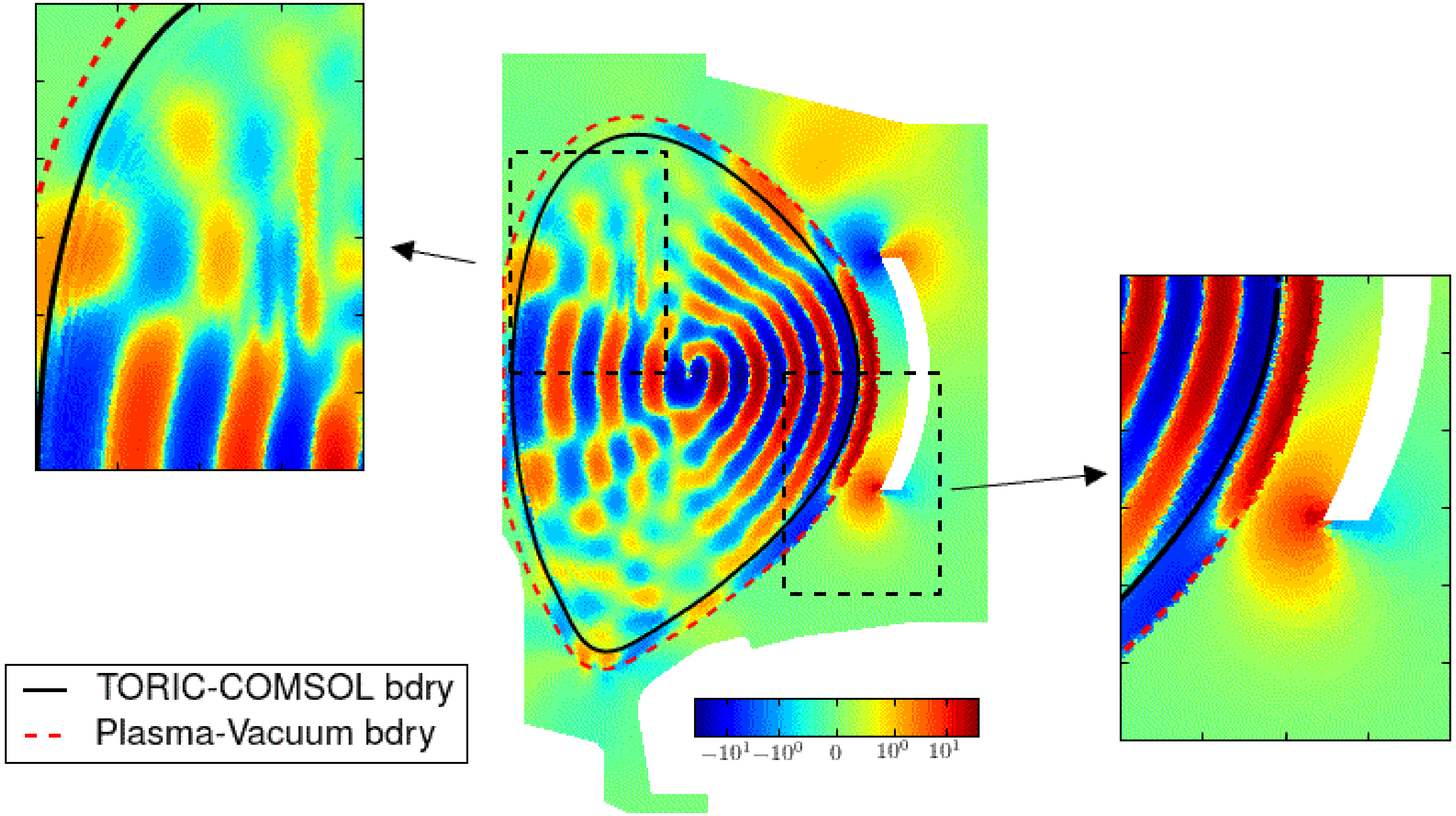

- Continuity of radial component is not given by construction and provides a way to verify the approach.
- Smoothly connected at TORIC/FEM boundary, but it is not at vacuum/plasma boundary.
- Consistent with a continuous dielectric at the former boundary, while it is not at the latter.

In D-(H) MH, the power is absorbed dominantly in the core

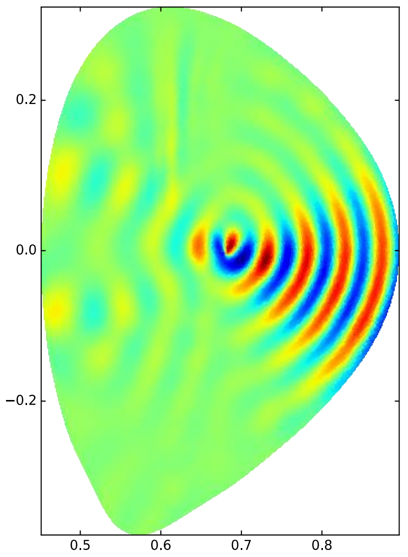

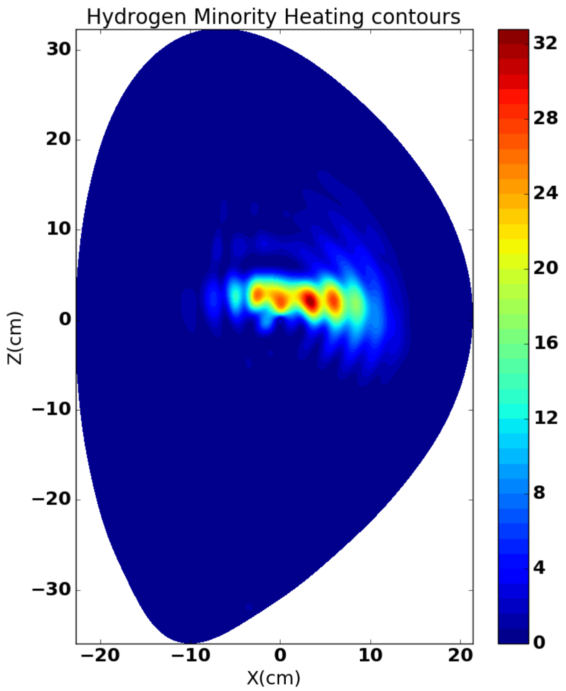

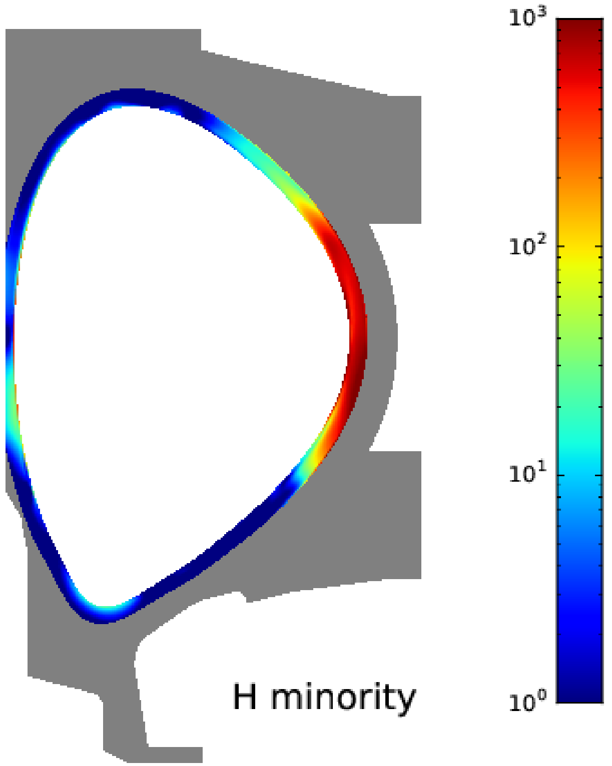

- D-(H) loading 16.1 Ω, power partition: 15% edge, 85% core.
  (note: Te_{SOL}= 15ev, which is low for C–Mod experiments)
- D-(3He) loading 14.5 Ω, power partition, 50% edge, 50% core.
- Loading is different than efficiency: power does not necessarily go into the core.
- In D-(3He), significant power lost in far SOL – possible source of far field RF sheath rectification

In D-(3He) MC, absorption in SOL increases due to weaker absorption

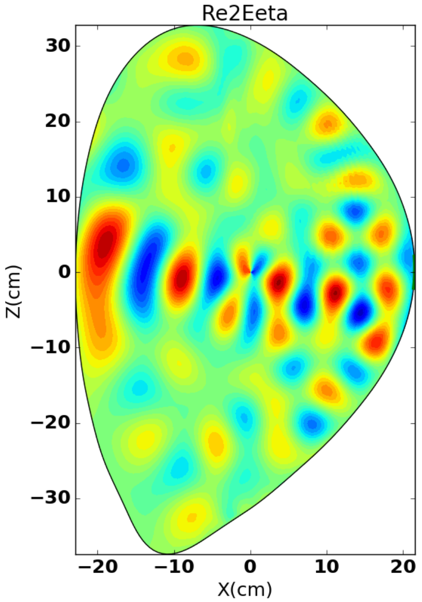

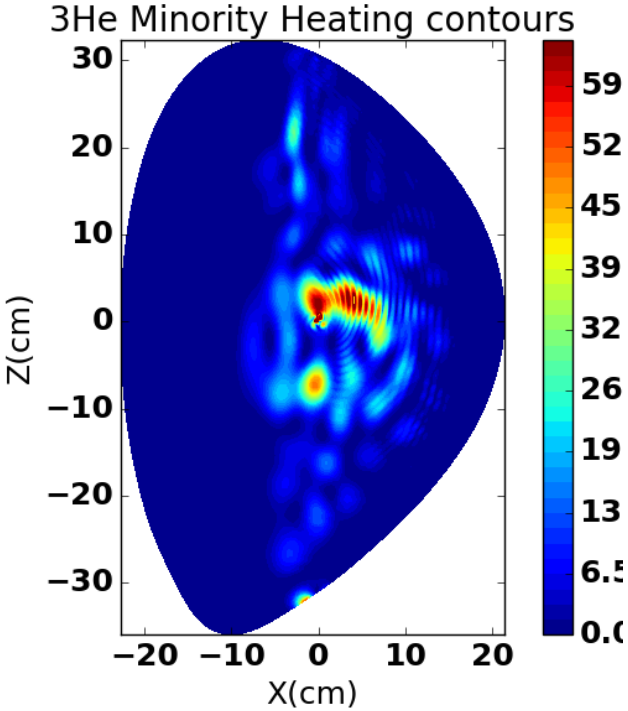

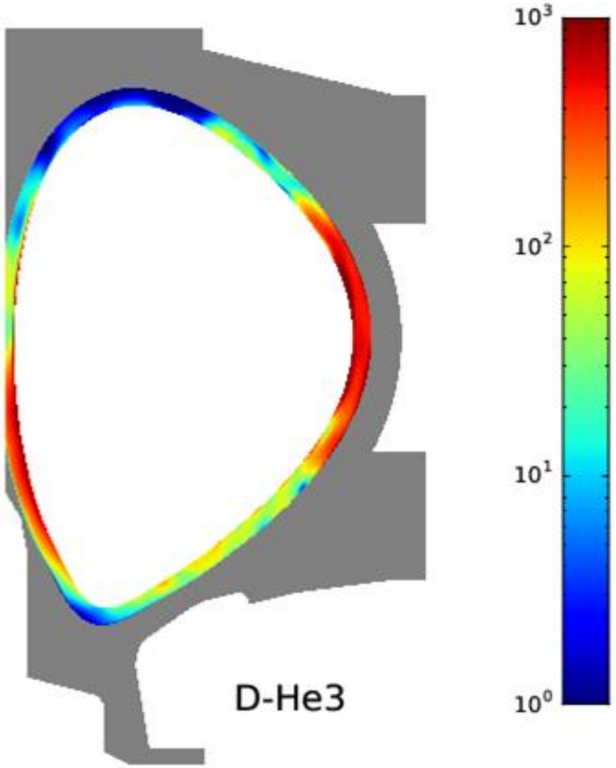

- D-(H) loading 16.1 Ω, power partition: 15% edge, 85% core.
  (note: Te_{SOL}= 15eV, which is low for C–Mod experiments)
- D-(3He) loading 14.5 Ω, power partition, 50% edge, 50% core.
- Loading is different than efficiency: power does not necessarily go into the core.
- In D-(3He), significant power lost in far SOL – possible source of far field RF sheath rectification

Our HIS formulation extends to 3D naturally

However, significantly larger resources are required

Geometry made by revolving previous poloidal cross section.

- 60 deg vessel section
- two strap antenna

Even a FE mesh, which is fine enough to resolve only the relatively long wavelength fast waves, yields a linear problem with ~5 M DoF.

Expecting 30 M ➔ 100 M DoF for resolving slow waves.

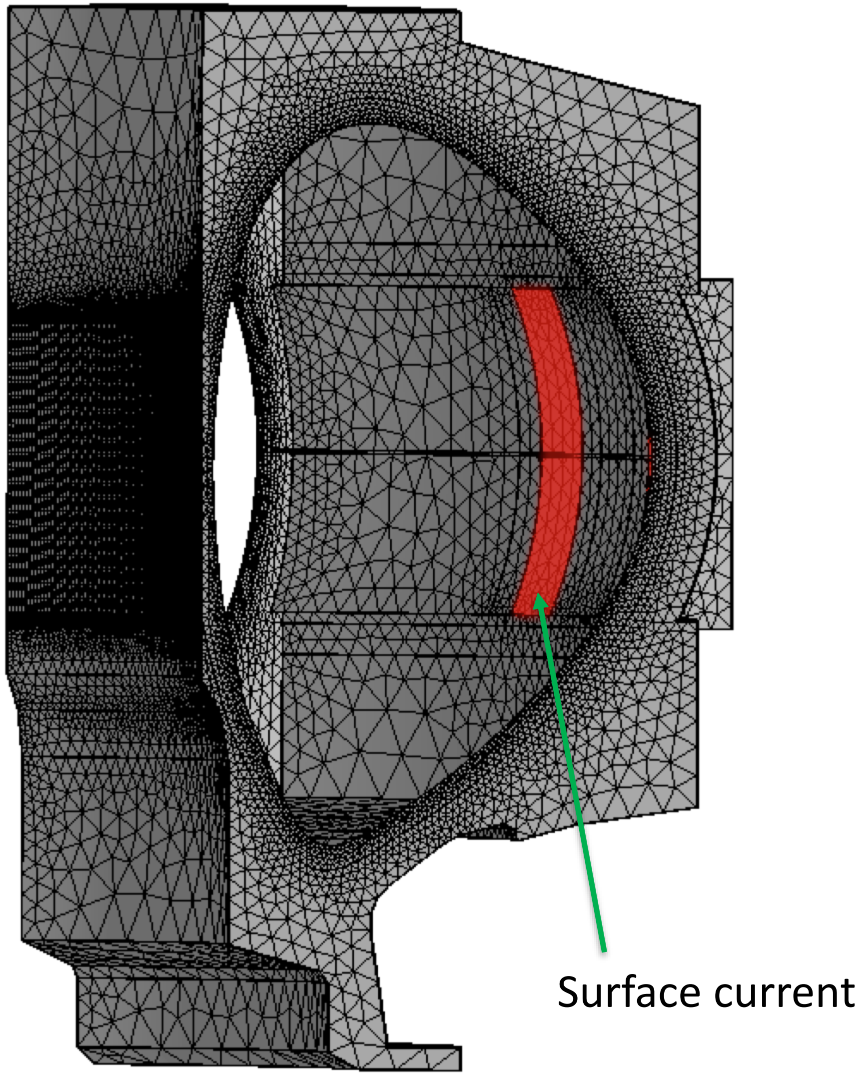

1342 x 2 solutions

SOL RF wave simulation built on Petra-M; an FEM modeling tool using the scalable MFEM library

- Scalable MFEM library
  - http://mfem.org/features

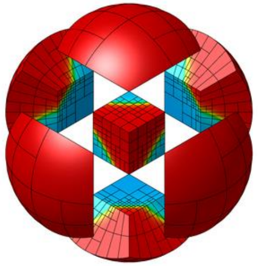

- Petra-M physics based FEM modeling interface

- Workflow management using πScope
  - http://piscope.psfc.mit.edu

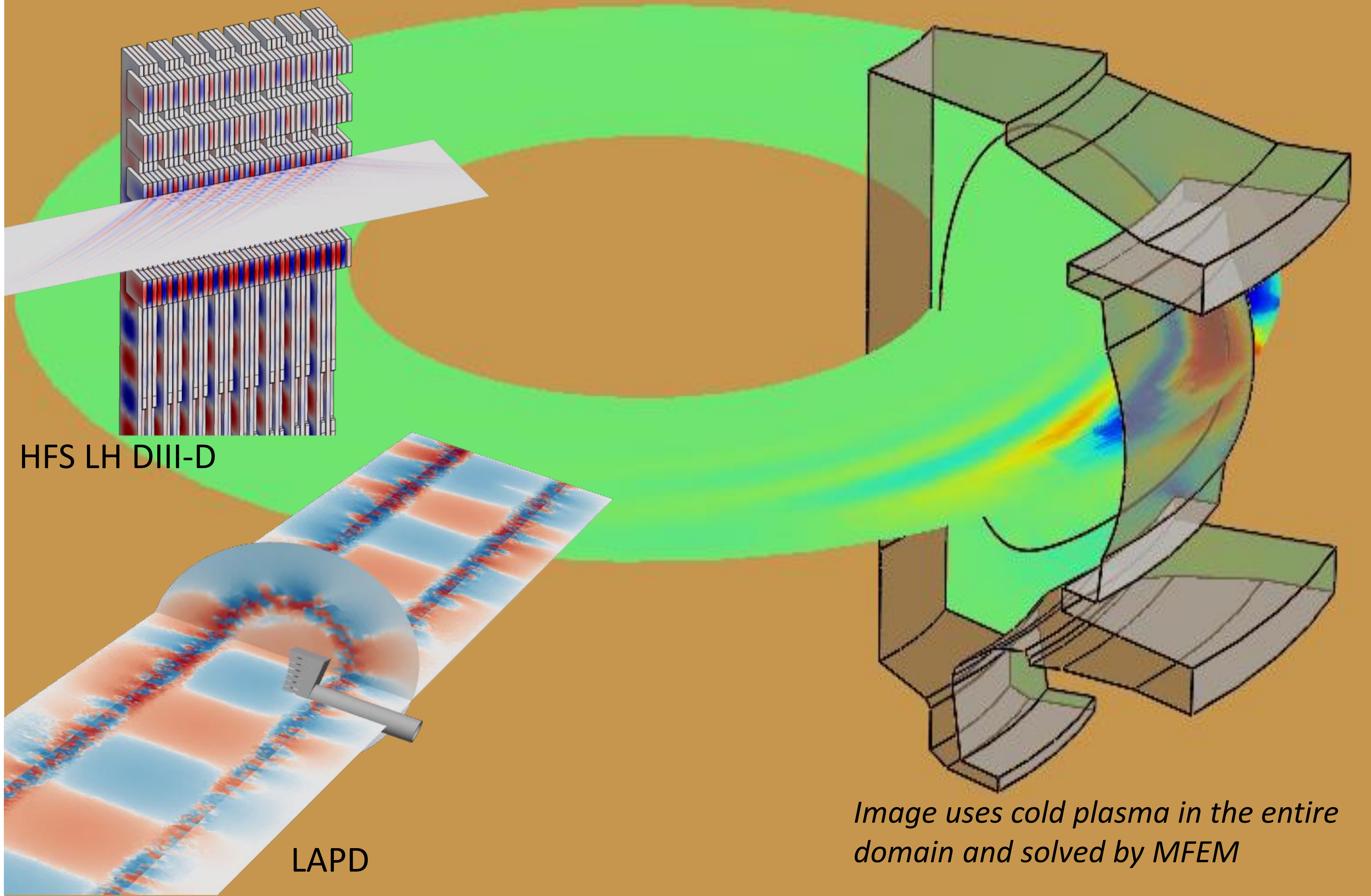

Image uses cold plasma in the entire domain and solved by MFEM

3D simulations using simply revolved 3D geometry indicates we need more realistic antenna structure

D-(H) case on Alcator C-Mod

Accurate toroidal spectrum can be essential for finding RF amplitudes ‘far’ from antenna[1].

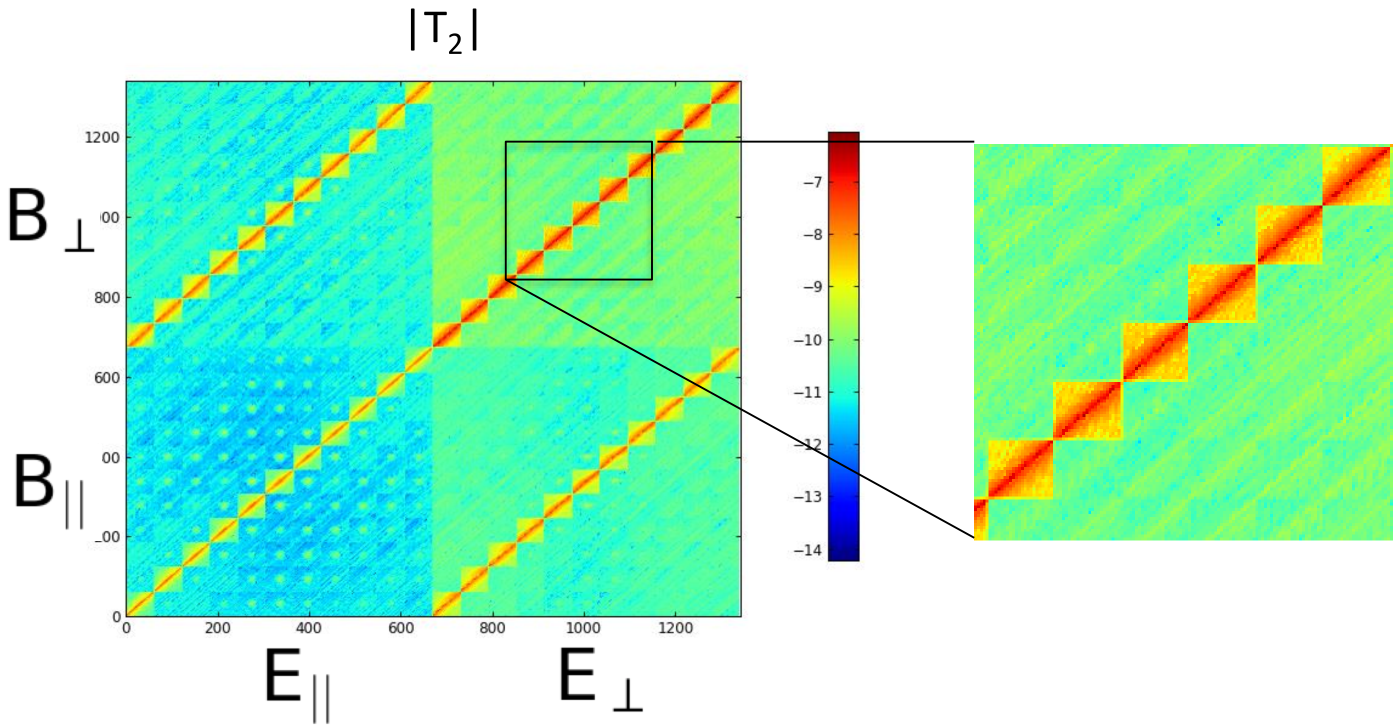

Midplane cut of low field side

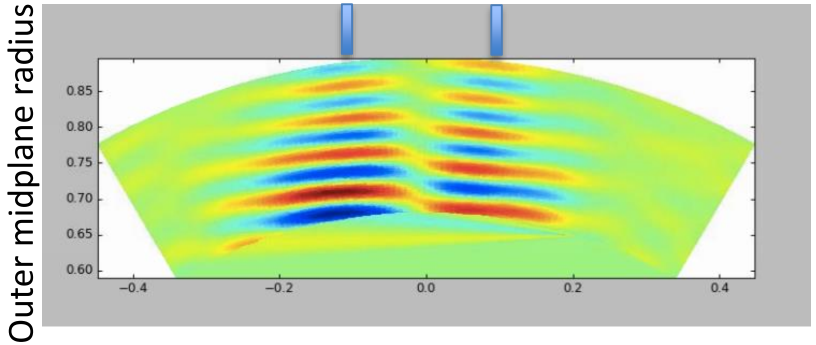

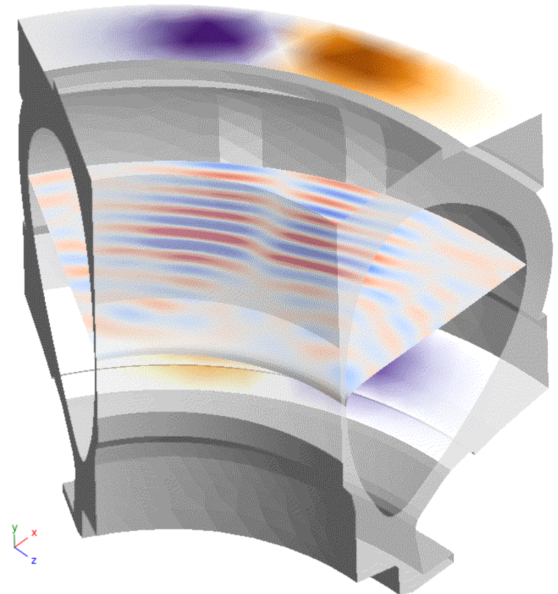

1) N. Tsujii, PhD thesis (2010)

J-port antenna RF geometry model built from engineering CAD drawing

Front

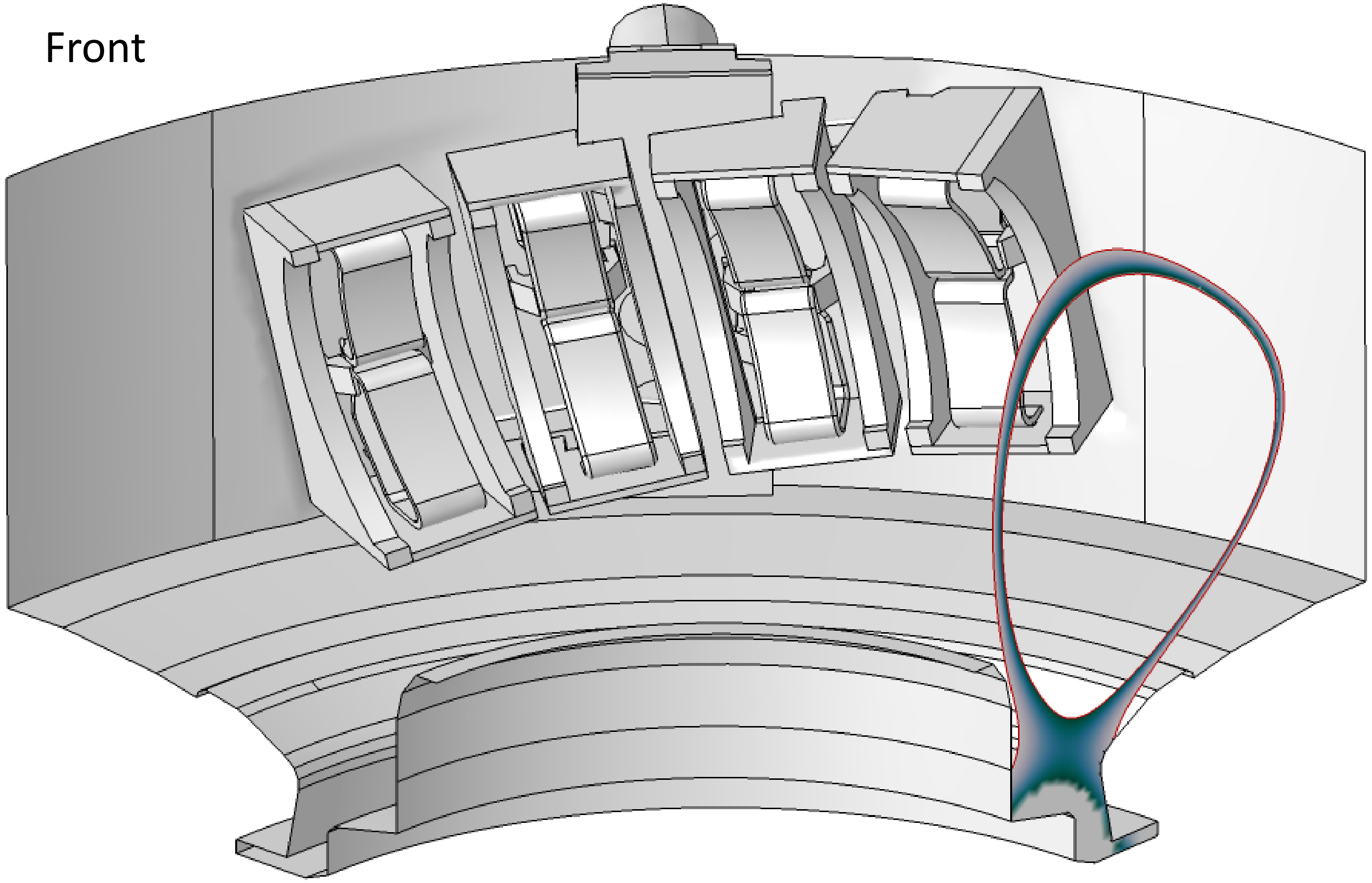

Back

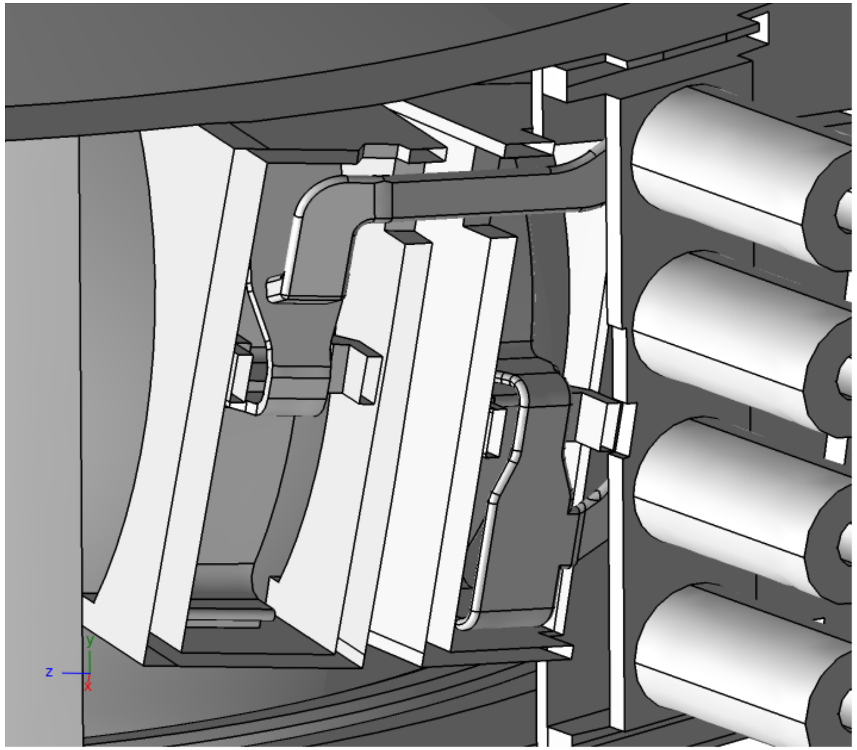

3D antenna structure and SOL plasma (diverted geometry is made from EFIT) is added

3D geometry introduces coupling among toroidal modes.

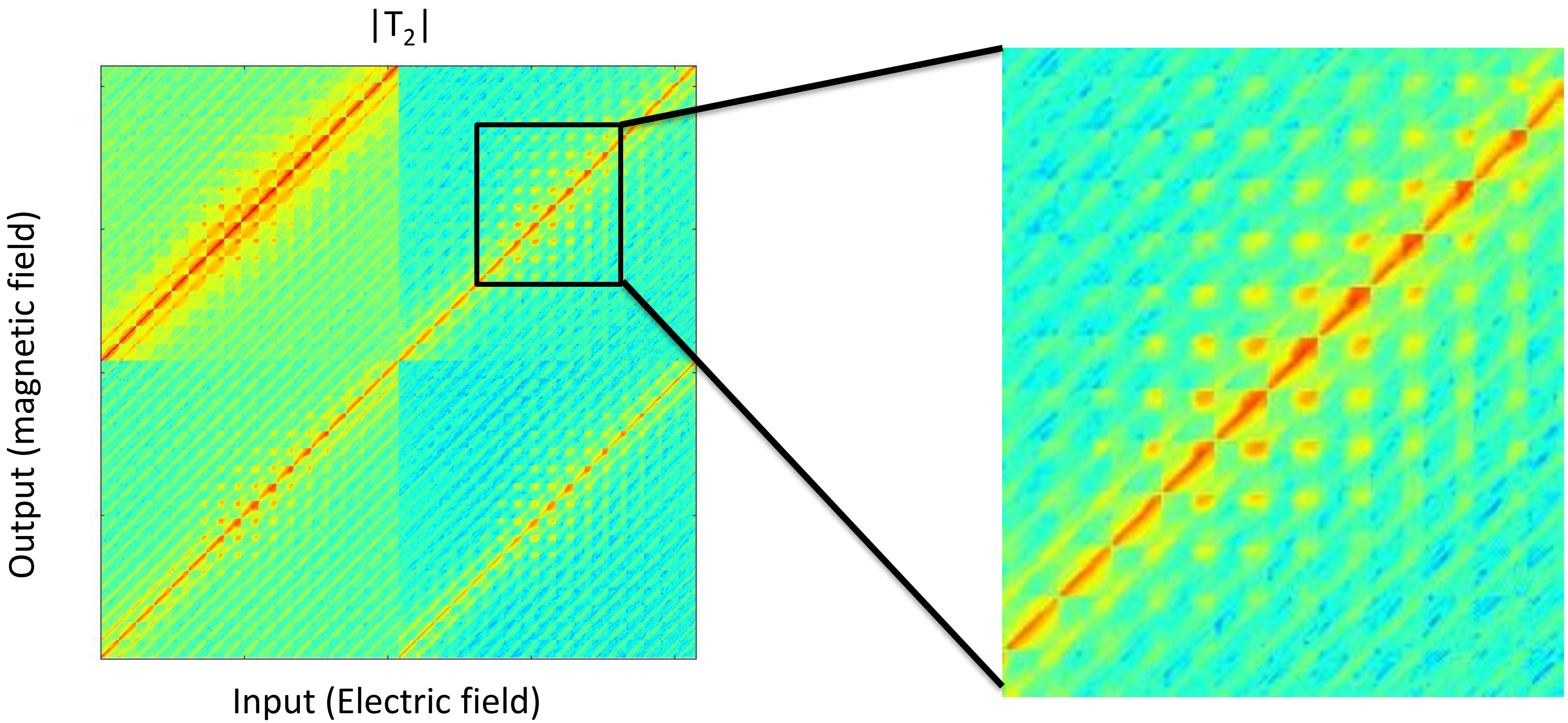

Different toroidal modes communicate each other via surface RF current on the antenna structure

Core-edge integrated solution for C-Mod field-aligned ICRF antenna

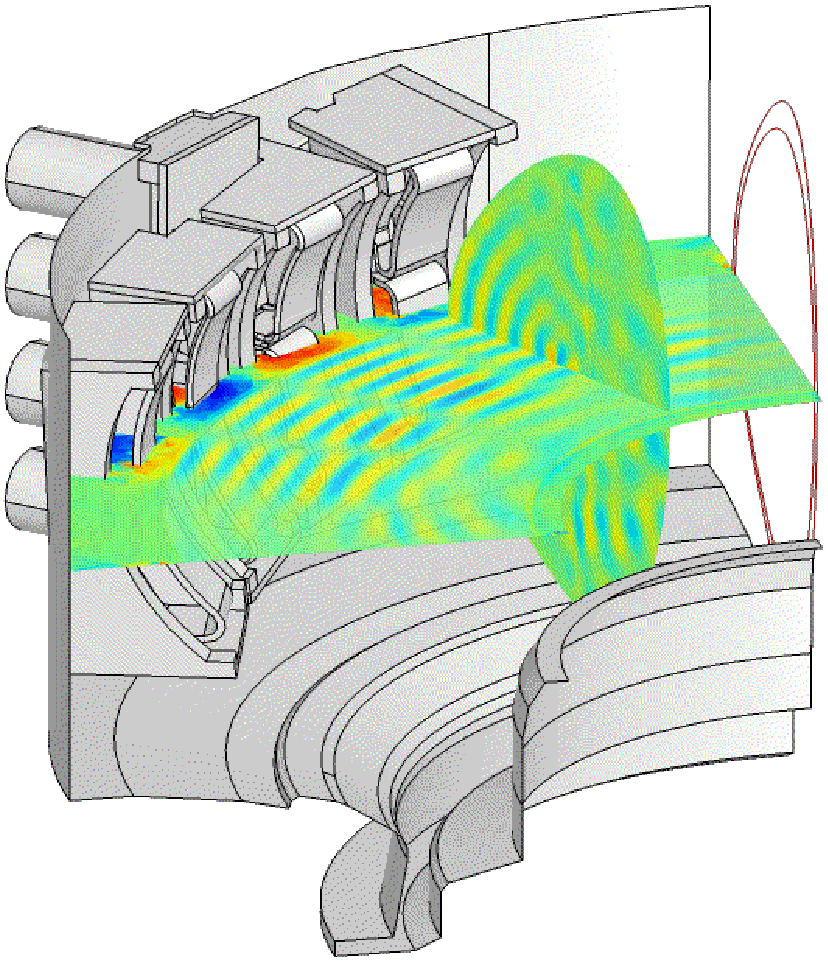

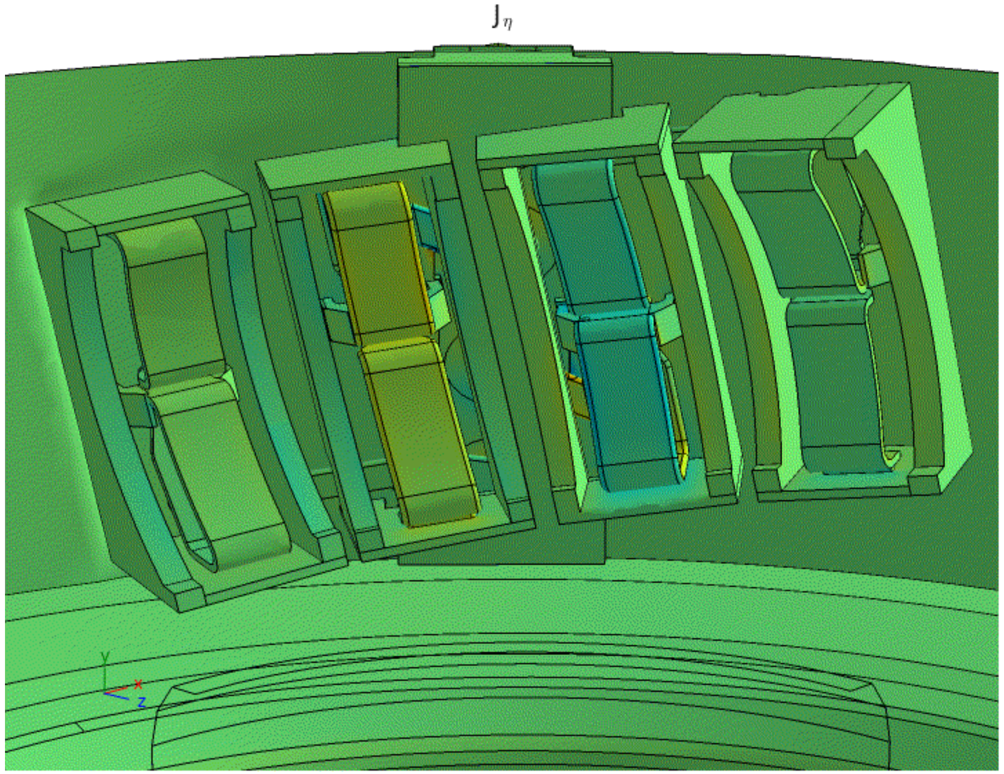

- Wave propagates smoothly from antenna to the core
- Surface currents indicates phasing is not exactly 0-pi-0-pi

HIS realized high degree of geometrical fidelity with hot core.

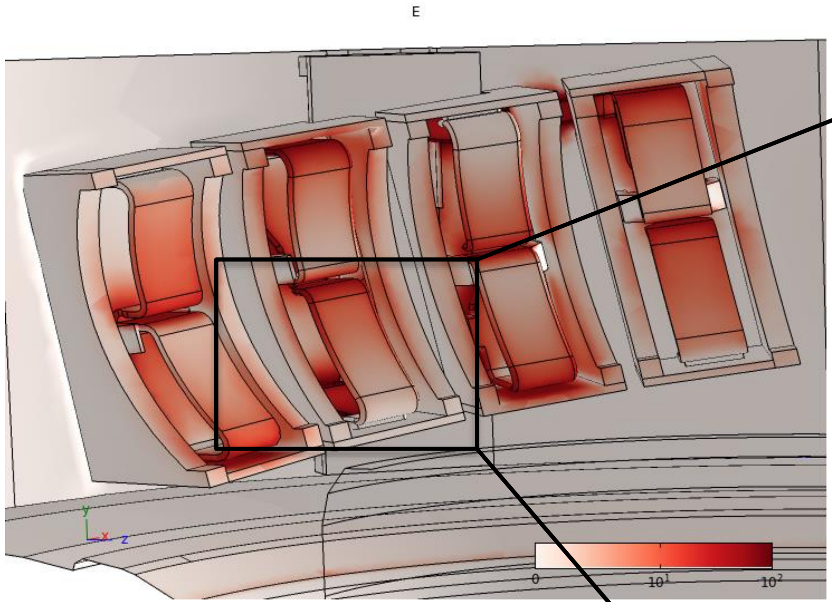

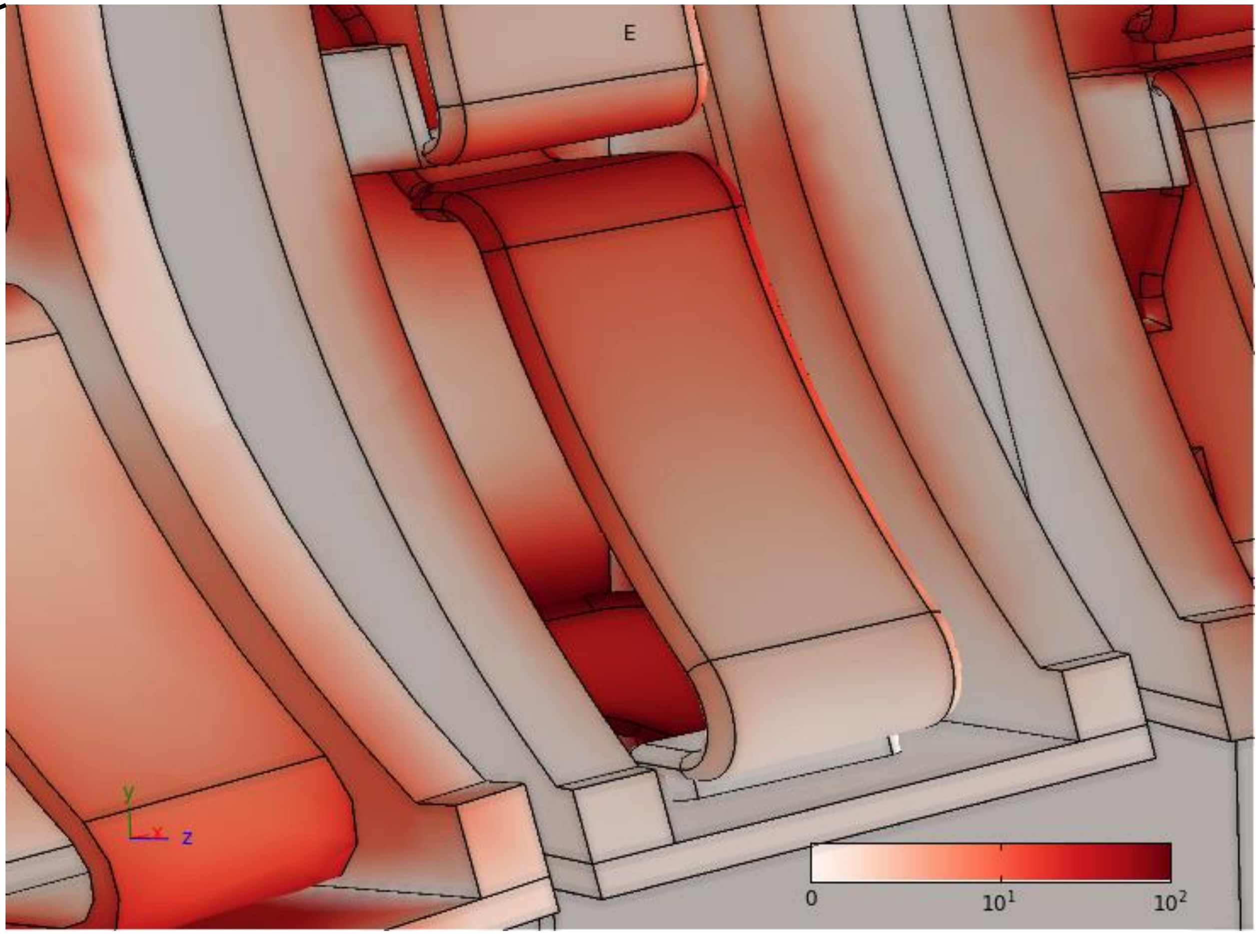

Validation is on-going using Alcator C-Mod experimental data

- RF voltage/current probes
- PCI diagnostics

LAPD, high density data points

Investigation of slow wave has begun

Slow wave excitation in the low density region near the antenna structure…

has very short wave length

produces nonlinear RF rectified potential

responsible for impurity regeneration

Work with J. Myra (Lodestar)

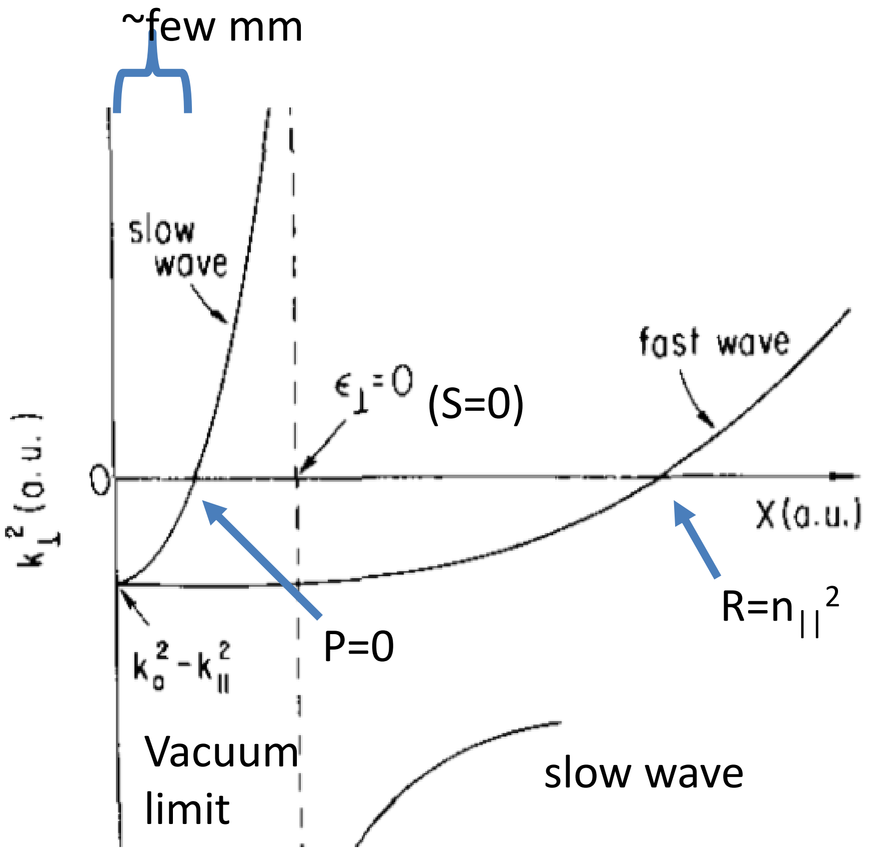

Fig.2 from Berro and Morales IEEE Trans. (1990).

1) J. R. Myra and D. A. D'Ippolito, Phys. Plasmas **22** , 062507 (2015)
2) H. Kohno, J.R. Myra, and D.A. D'Ippolito, Phys. Plasmas **22**, 072504 (2015)

Investigation of slow wave has begun

Slow wave excitation in the low density region near the antenna structure

- has very short wave length
- produces nonlinear RF rectified potential
- responsible for impurity regeneration

Work with J. Myra (Lodestar)

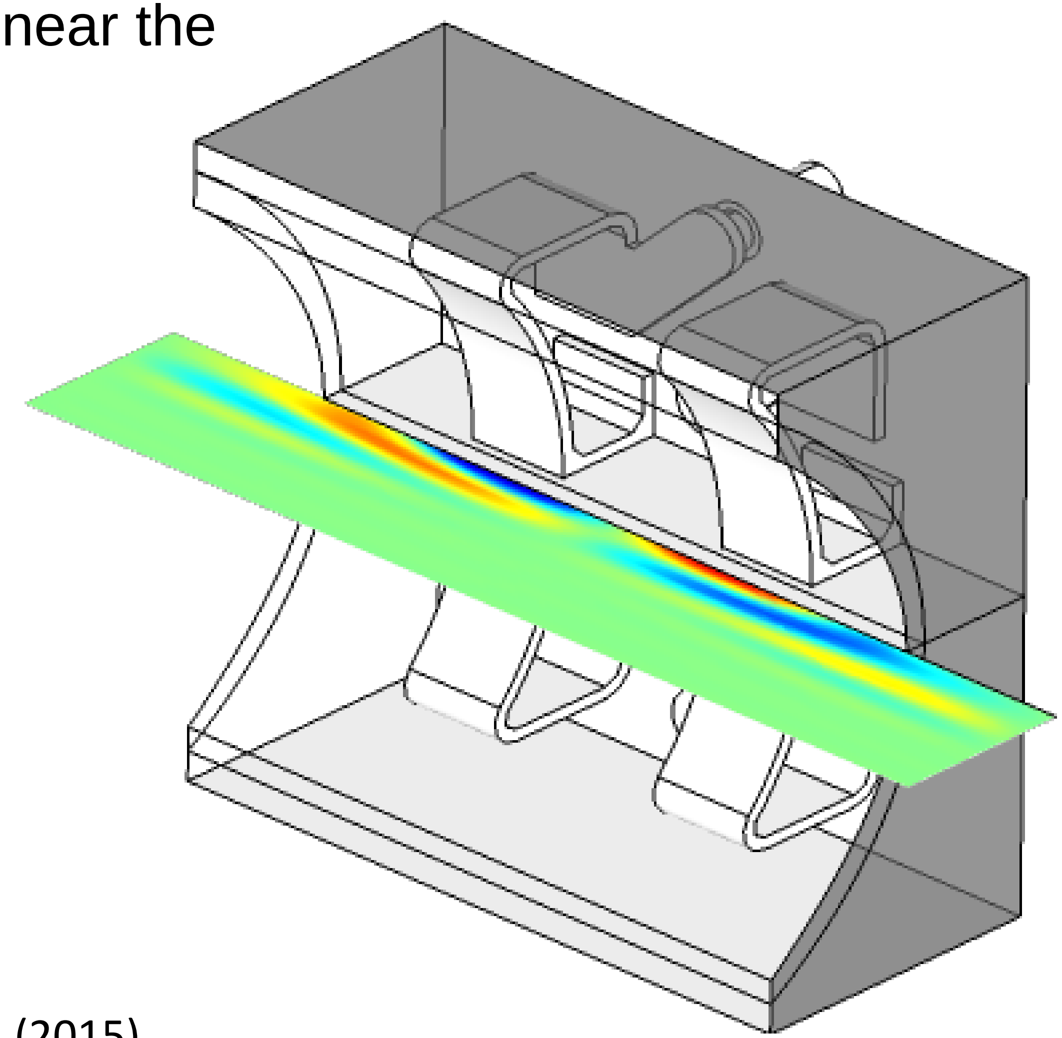

1) J. R. Myra and D. A. D'Ippolito, Phys. Plasmas **22** , 062507 (2015)
2) H. Kohno, J.R. Myra, and D.A. D'Ippolito, Phys. Plasmas **22**, 072504 (2015)

Investigation of slow wave has begun

Slow wave excitation in the low density region near the antenna structure

- has very short wave length
- produces nonlinear RF rectified potential
- responsible for impurity regeneration

Work with J. Myra (Lodestar)

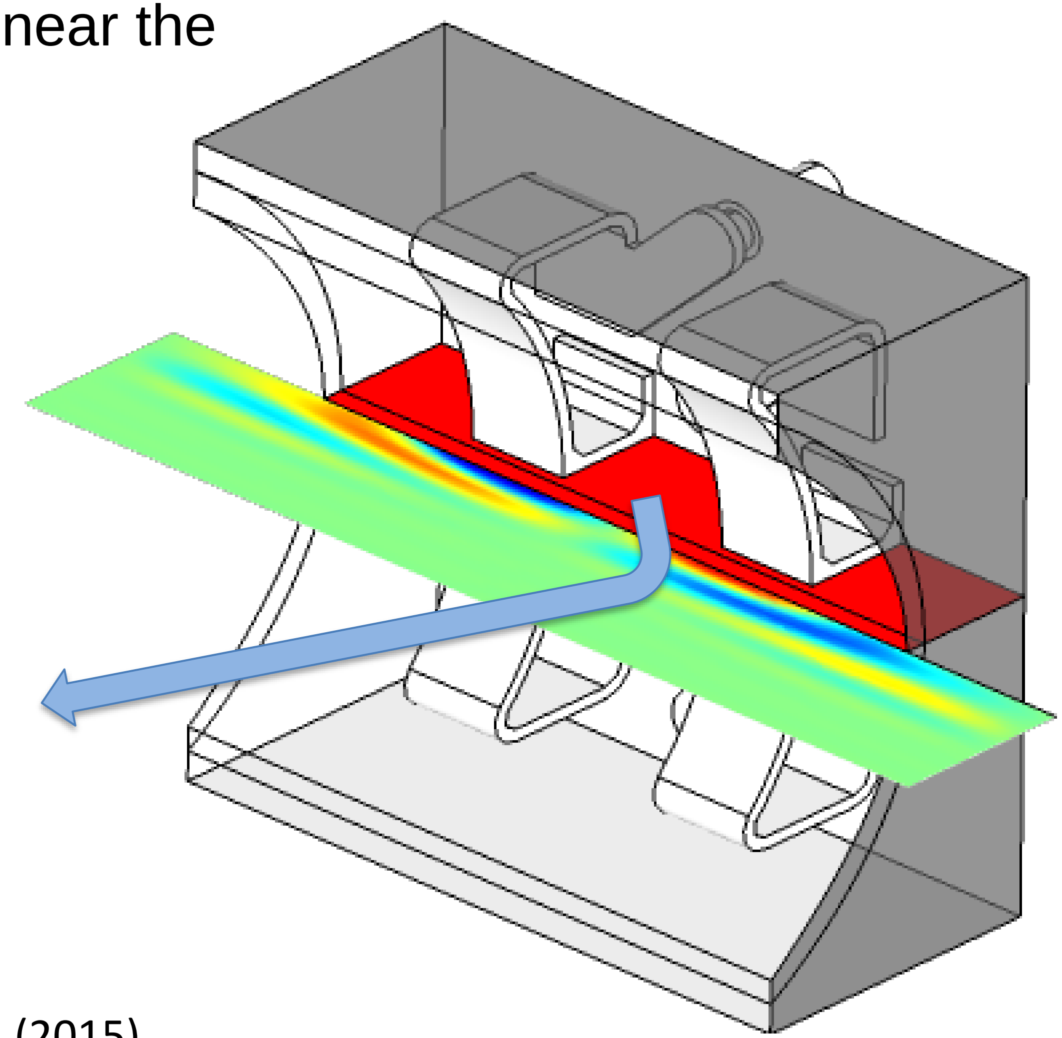

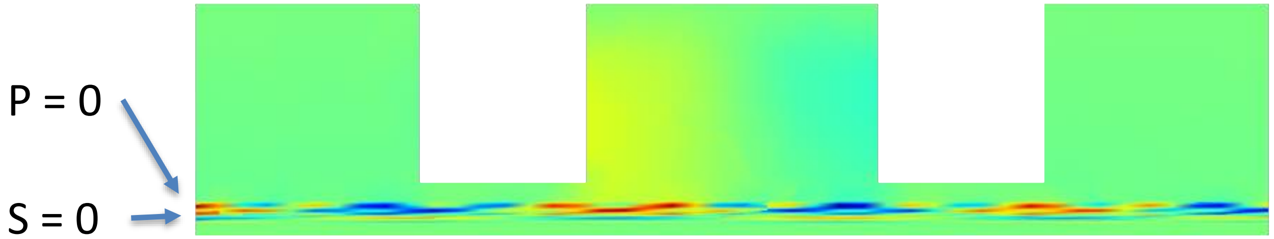

1) J. R. Myra and D. A. D’Ippolito, Phys. Plasmas **22** , 062507 (2015)

2) H. Kohno, J.R. Myra, and D.A. D'Ippolito, Phys. Plasmas **22**, 072504 (2015)

Possible application to EAST

EAST B-antenna

Unstructured geometry mesh was generated (3M DoFs for EM)

What we need…

- Equilibrium
- 1D Core temperature and density profiles (for TORIC)
- 2D SOL density (ideally temperature too) profiles

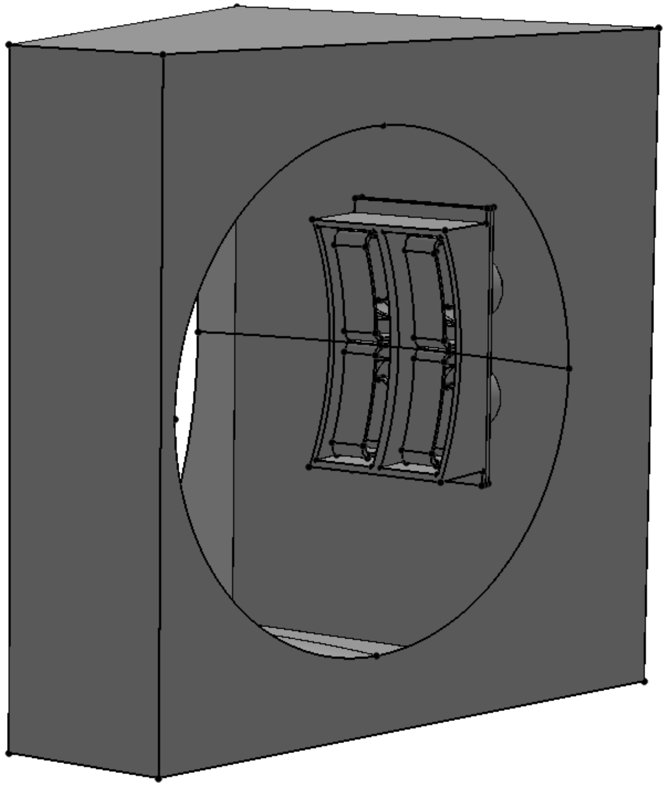

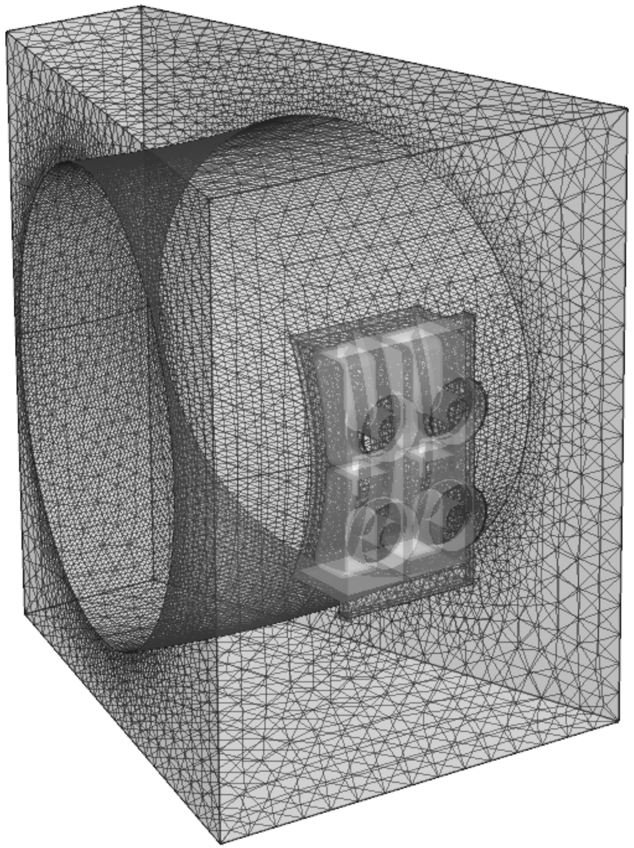

Conclusions

A new RF modeling capability permits exploration of core – edge interactions in many areas

- Technique applies to any full wave RF simulation in any frequency regime.
- Builds upon existing code infrastructure, algorithms and methods.
- Newly developed SOL FEM simulation built on the scalable MFEM library
- Integrates for the first time, antenna coupling, SOL propagation with realistic geometry, and hot core plasma.

A step towards whole device scale RF modeling

RF sheath models

Core Fokker-Planck models

SOL fluid and turbulence models

Impurity generation and transport models

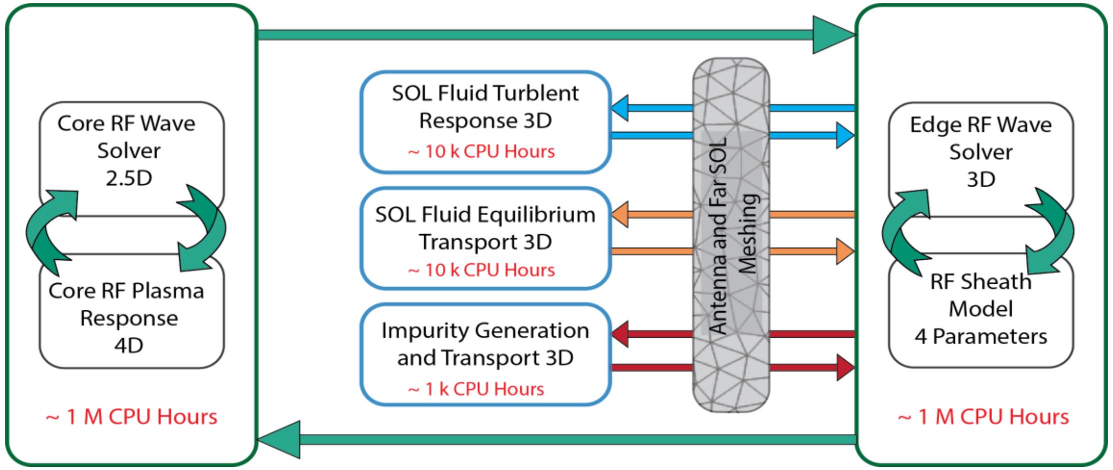

HIS approach adopted by "Center for Integrated Simulation of Fusion Relevant RF Actuators"

How to stitch to two regions…

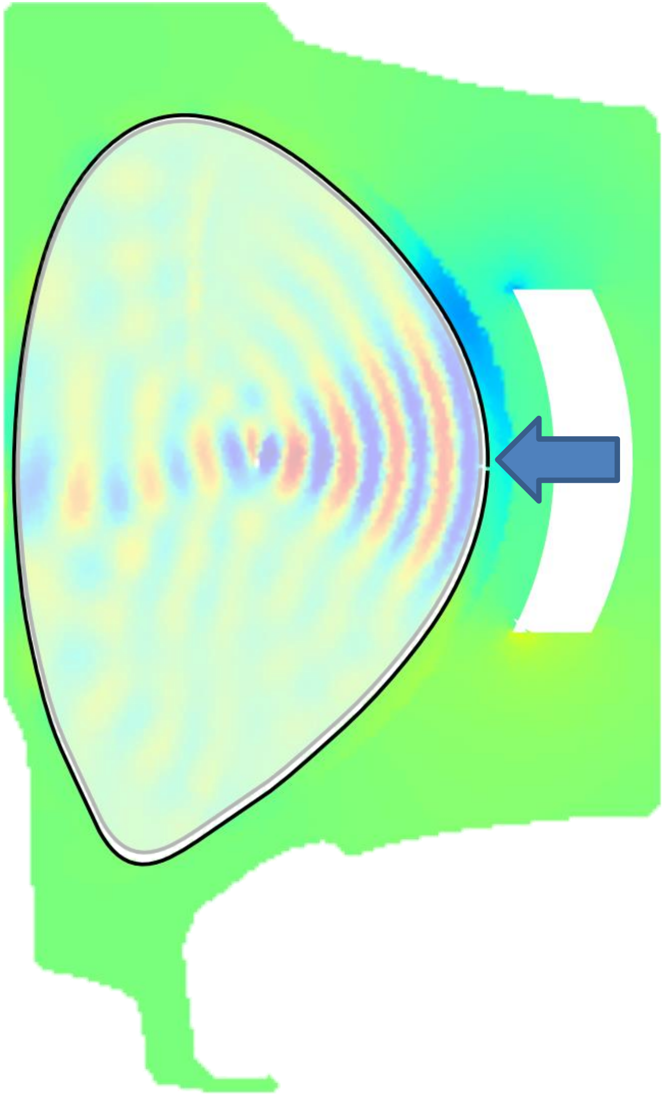

Let's follow the power flow….

- Antenna current inject the RF power to SOL

How to stitch to two regions…

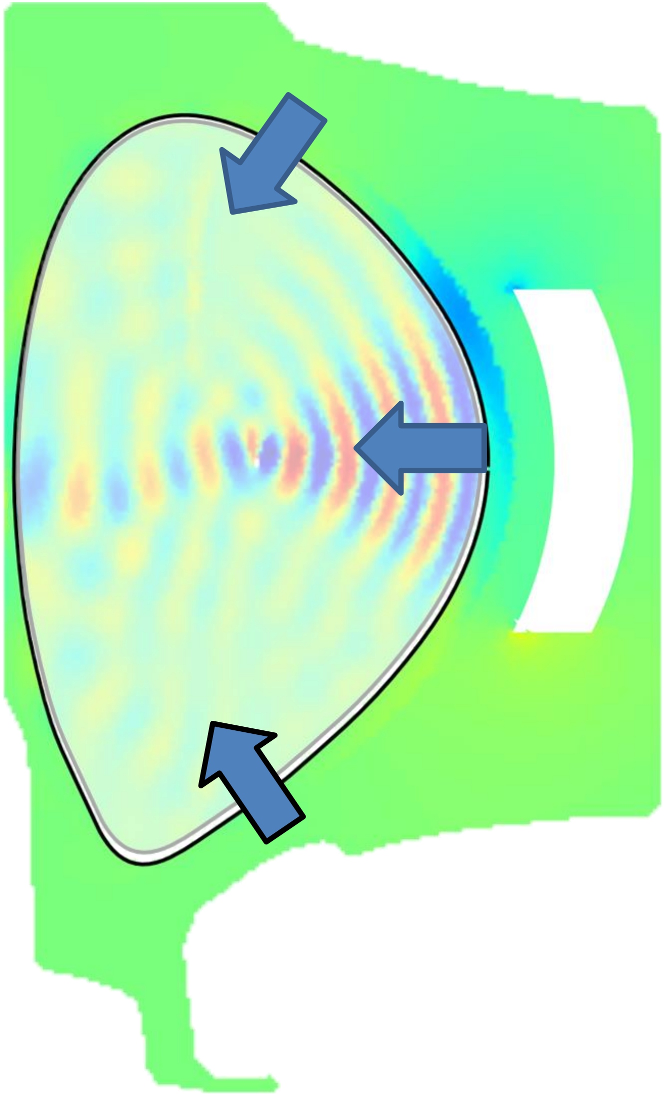

Let’s follow power flow….

- Antenna current inject the RF power to SOL
- The RF power goes through the SOL and across the connecting boundary to enter the core

How to stitch to two regions…

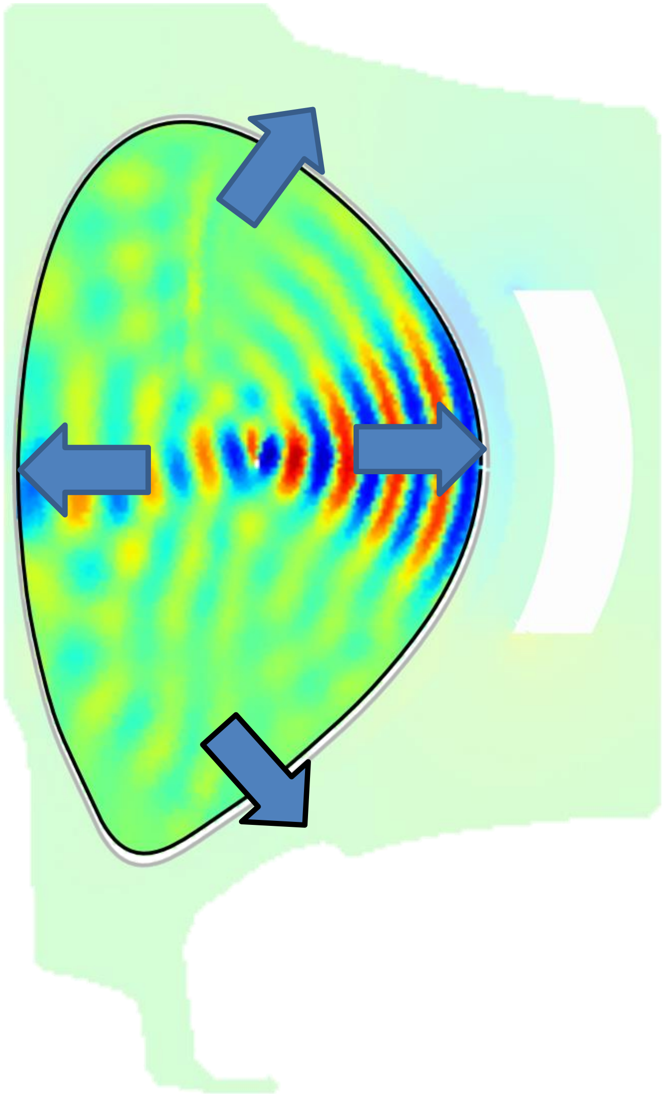

Let's follow power flow….

- Antenna current inject the RF power to SOL
- The RF power goes through the SOL and across the connecting boundary to enter the core
- The power not being absorbed comes out to SOL

How to stitch to two regions…

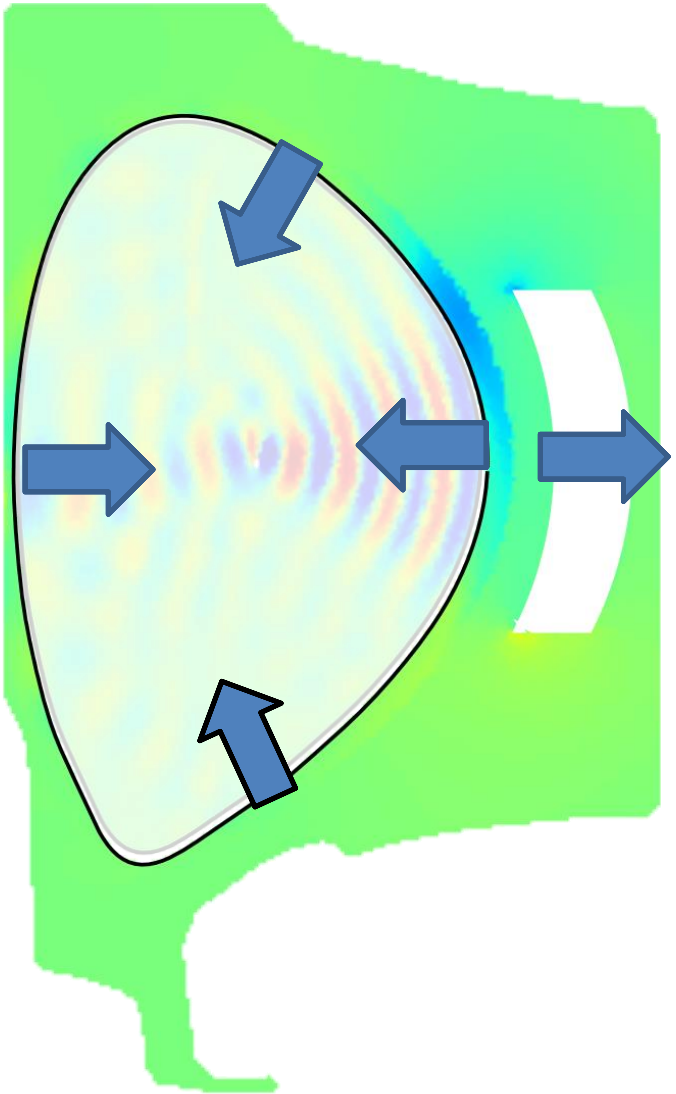

Let's follow power flow….

- Antenna current inject the RF power to SOL
- The RF power goes through the SOL and across the connecting boundary to enter the core
- The power not being absorbed comes out to SOL
- The power is sent back to core or to the transmitter